The Biophysicist

A Practical Guide to Fluorescence Temporal and Spatial Correlation Spectroscopy

E. Pandzic[1]*, R. M. Whan

[1]Biomedical Imaging Facility, Mark Wainwright Analytical Centre, University of New South Wales Sydney, Kensington, 2052, Australia.

ABSTRACT The aim of this article is to introduce the basic principles behind the widely used microscopy tool: fluorescence fluctuation correlation spectroscopy (FFCS). We present the fundamentals behind single spot acquisition (FCS) and its extension to spatiotemporal sampling, which is implemented through image correlation spectroscopy (ICS). The article is an educational guide that introduces theoretic concepts of FCS and some of the ICS techniques, followed by interactive exercises in MATLAB. There, the learner can simulate data time series and the application of various FFCS techniques, as well as learn how to measure diffusion coefficients, molecular flow, and concentration of particles. Additionally, each section is followed by a short exercise to reinforce learning concepts by simulating different scenarios, seek verification of outcomes, and make comparisons. Furthermore, we invite the learner throughout the article to consult the literature for different extensions of FFCS techniques that allow measurements of different physicochemical properties of materials. Upon completion of the modules, we anticipate the learner will gain a good understanding in the field of FFCS that will encourage further exploration and adoption of the FFCS tools in future research and educational practices.

KEY WORDS fluorescence fluctuation correlation spectroscopy; concentration and dynamics characterisation; quantitative microscopy; image simulation and analysis

I. INTRODUCTION

It has been nearly half a century since the first papers established the foundations on fluorescence correlation spectroscopy (FCS) were reported (1, 2). In its basic form, FCS (Fig 1A,B) was used to measure the chemical reactions and diffusion coefficients of an ensemble of particles in a steady state, by measuring the temporal thermal fluctuation in particle local concentrations within a focused beam of light. This fundamental work has been further developed alongside the improvement in modern confocal microscopes to result in fluorescence fluctuation correlation spectroscopy (FFCS) that permits dual-color colocalization analysis (3) to measure proteins conformational states, protein–protein interactions, dynamics, and kinetics (4–8). For detailed reviews on FCS extensions and applications, we direct the readers to more in-depth reviews (9, 10).

Modern laser scanning confocal microscopes (LSCM) have become a major tool in the researchers toolbox and now provide better signal to noise data, faster imaging rates and sampling in several dimensions (x, y, z, t, λ). Not surprisingly, this influenced the extension of FCS into spatial sampling, or image correlation spectroscopy (ICS). Some of the

"*" corresponding author

Received: 29 December 2019
Accepted: 1 September 2020
Published: 17 February 2021

FFCS techniques covered in this guide

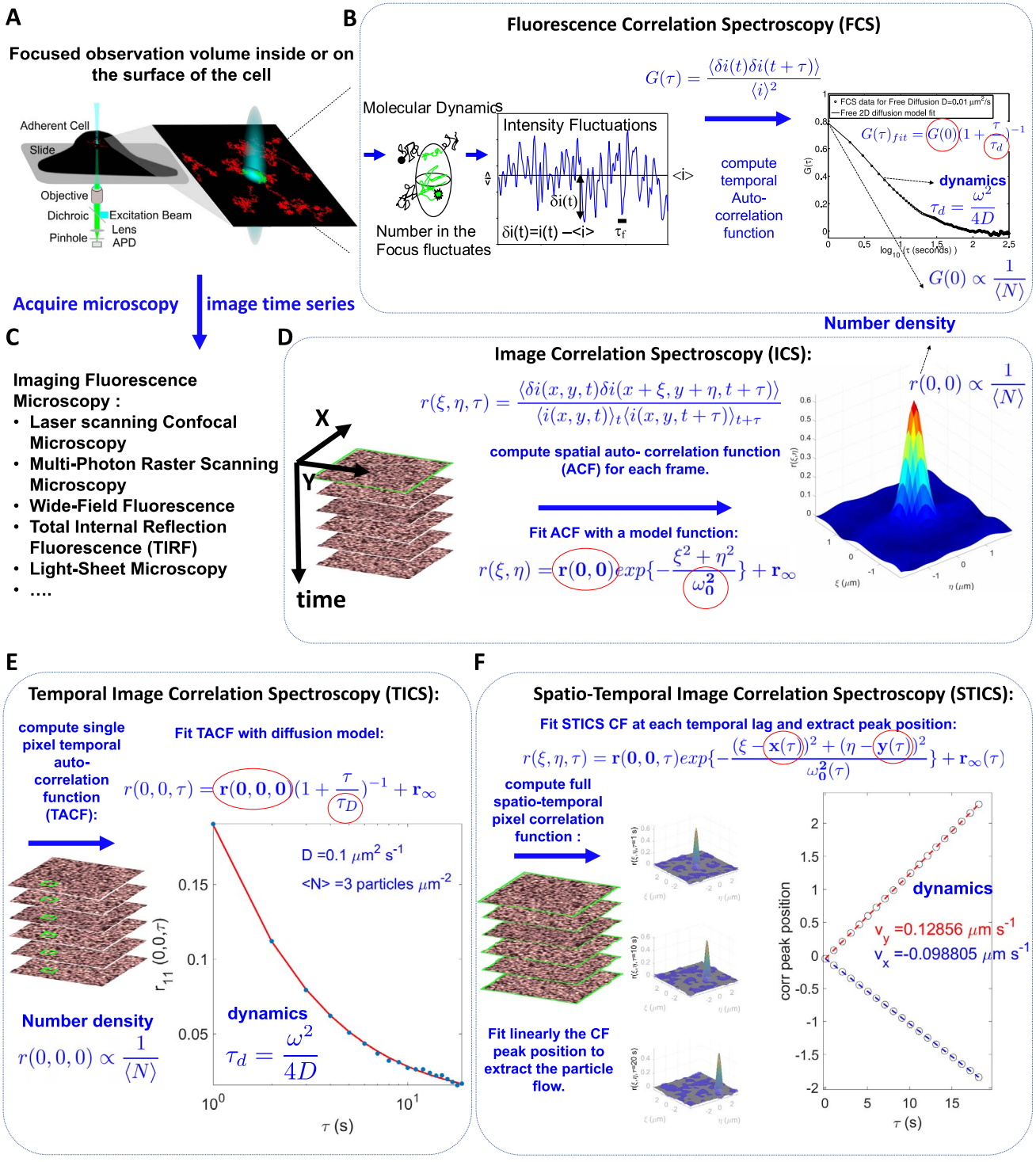

Fig 1. (A) In the FCS experiment, an excitation volume is focused within cell region of interest and fluorescent molecules are illuminated as they transit through. (B) FCS measures the fluorescence fluctuations in time from an observation volume. The ACF is fitted with characteristic model to extract the particle dynamics (diffusion or flow) and density. (C) Different fluorescence imaging microscopy modalities used to generate data that can be used for ICS analysis. (D) In ICS, a single image is correlated with itself to produce an ACF that is fitted to a 2D Gaussian model for number density characterization. (E) In TICS, a single pixel temporal intensity fluctuation is characterized by temporal ACF calculation and fit to obtain particle number density and dynamics. (F) STICS involves full spatiotemporal ACF to obtain a CF that translates in temporal lags according to the dominant flow in the image data. The fitting at each temporal lag, with 2D Gaussian, and extracting the peak position of CF allows for particle flow characterization.

first ICS experiments (Fig 1C,D) were applied to measure the aggregation and concentration of membrane receptors (11–16) and with this new capability came the need to characterize the protein colocalization from dual-channel microscope images, which, in turn, led to the development of image cross-correlation spectroscopy (ICCS) (17–20). As these ICS techniques were applied to more systems, it was realized that some systems exhibited relatively slow diffusion dynamics and required a different approach, and a frame-to-frame temporal correlation was established to allow parallelization of FCS. This extension was named temporal ICS (TICS; Fig 1E) or (17, 18, 21).

The capacity of TICS to obtain a single pixels temporal intensity fluctuation within a time series was an exciting one, and it was not long before a full spatiotemporal image correlation, (STICS; Fig 1F) allowed for the accurate measurement of molecular flow (22, 23), protein cofluxing (24–27), organelle dynamics (28, 29), and cellular migration (30, 31). These few examples of applications are testaments to the growth of the FFCS field and the capacity to provide novel insight into molecular dynamics.

Herein, we describe the theoretic background of FFCS, with emphasis on fitting models and determining the diffusion coefficient, molecular flow, and particle concentrations. We introduce the simulation and analysis scripts and proceed with exercises in FCS, ICS, TICS, and STICS. We conclude with a brief discussion inviting the readers to consult further literature where some of the new and specialized adaptations of FFCS approaches that shine new light in fundamental and applied sciences.

II. THEORY

The aim of this section is to introduce the reader to some theoretic concepts related to FFCS techniques and how the fluorescence fluctuations measured from a single probing volume (FCS) or multiple pixel fluctuations (ICS) can be used to recover some useful information about the system, such as molecular concentrations, diffusion coefficients, molecular fluxes, and more. While it is highly recommended that the reader consult some of the literature (1, 2, 9) to find out more about underlying development of equations presented here, we will keep the presentations at the introductory level. Appendix A contains further developments showing how the combination of Eqs. 1 and 2 lead to a free diffusion fit model. It is fundamental that the reader grasps the origin of some of the fitting models and how they link to the system's parameters, as well as modality of spatiotemporal sampling. The basic idea behind any FFCS technique is that particles within a system undergo local fluctuations in concentration above and below their average constant value in space and time. These fluctuations, which can be due to particle diffusion, flow, or chemical reactions, are observable if we use a sufficiently small measurement volume, typically on the order of a femtoliter. In the experimental realization of the first FCS experiment, a beam of focused light was used to excite a local subvolume in which particles would fluoresce when within the volume. As particles move in and out of beam, they would produce fluorescence fluctuations in time, which could be correlated to obtain a characteristic autocorrelation function (ACF) that characterizes this ensemble of the particles. An important concept in FFCS is that the system is in steady state, either equilibrium or nonequilibrium, and that if one observes the fluorescence fluctuations over long enough experimental time, then the time average is equivalent to the ensemble average of the system, by the ergodicity principle. Let us define the temporal average of the measurement within a subvolume as $\langle F \rangle$ and let $\delta F(t) = F(t) - \langle F \rangle$ be the fluctuation of fluorescence at time t. A single fluctuation in time does not tell us much about the ensemble of particles producing it, but if we take those fluctuations and correlate them in time (or space as in ICS), we generate a fluorescence fluctuation ACF, $G(\tau) = \langle \delta F(t) \delta F(t+\tau) \rangle$. Here, symbols $\langle \ldots \rangle$ signify that averaging over a long time period, much longer than the characteristic time of single fluctuation produced by particle movement. Now that we introduced $G(\tau)$, it is valid to ask how a fluorescence fluctuation in small

observation volume, dV relates to the fluctuation of particle concentration and ultimately to the underlying dynamics of particles. First, let us define the fluorescence observed from the small observation volume by using some system and microscope parameters: $dF_i(r,\ t) = g_i I(r) c_i(r,\ t) dV$, where g_i accounts for fluorophore's quantum efficiency and absorbance, $I(r)$ is the spatial distribution describing the extent of observation volume, $c_i(r,\ t)$ is the concentration of ith dynamical species defined in space and time. With this information, we can define the relation between the fluorescence and concentration fluctuation of the ith dynamical species: $\delta F_i(t) = g_i \int_{-\infty}^{+\infty} I(r)\delta c_i(r,t)dr$. Then, for a system of M fluorescent dynamical species:

$$G(\tau) = \frac{\sum_{i=1}^{M}\sum_{j=1}^{M}\langle \delta F_i(0)\delta F_j(t)\rangle}{\left(\sum_{i=1}^{M}\langle F_i(t)\rangle\right)^2} = \frac{\sum_{i=1}^{M}\sum_{j=1}^{M} g_i g_j \int_{-\infty}^{+\infty} I(r)I(r')\langle \delta c_i(r,0)\delta c_j(r',\tau)\rangle dr dr'}{\left(\int_{-\infty}^{+\infty} I(r)dr \sum_{i=1}^{M} g_i\langle c_i\rangle\right)^2} \quad (1)$$

where i and j are indexes for particle species i and j. In Eq. 1, what is essential is that the left-hand side, $G(\tau)$ is directly proportional to the density–density fluctuation of particles, $\langle \delta c_i(r,0)\ \delta c_j(r',0)\rangle$ within the observation subvolume. All the other parts of that equation consider the fluorophore's quantum efficiency and absorption, observation volume spatial extent, and denominator of the equation for normalization purposes. The second piece of information we need is to connect the density–density fluctuations to the underlying system parameters, such as particles diffusion coefficient or flowing speed, as well as kinetic rates, in case the system undergoes equilibrium chemical reaction. Depending on the dynamics and kinetics involved in controlling the particle populations, we can describe the concentration of M particles species by using a system of convection–diffusion–reaction partial differential equations:

$$\frac{\partial c_i(r,t)}{\partial t} = D_i\nabla^2 c_i(r,t) - V_i\frac{\partial c_i(r,t)}{\partial x} + \sum_{j=1}^{M} T_{ij}\delta c_j(r,t) \quad (2)$$

What is important to grasp from Eq. 2 is that the left-hand side expresses the time evolution of particles concentration of ith species in time within small system subvolume and how it depends on various dynamics and kinetics, as described on the right-hand side of the equation. The first term on the right-hand side describes the particles diffusion of species i, D_i, the second term describes the particles flow, V_i, and the final term describes the changes in concentration, c_i of ith species due to a chemical reaction rate, T_{ij} influencing concentrations of other M-1 species, δc_j. Depending of what type of dynamics and kinetics regulate the particles concentration in the system, we can choose which components of Eq. 2 are important and use in the fitting equation model to describe the experimental ACF $G(\tau)$.

For instance, if one assumes that particles undergo only diffusion and use only the first terms of Eq. 2 and plug the solution to the system of equations for M species, into Eq. 1, then one can find expression for the ACF:

$$G(\tau) = \frac{1}{\pi\omega_0^2}\frac{\sum_{i=1}^{m}\langle c_i\rangle q_i^2 \times \left(1+\frac{\tau}{\tau_{\mathbf{D_i}}}\right)^{-1}}{\left(\sum_{i=1}^{M}\langle c_i\rangle q_i\right)^2} \quad (3)$$

where q_i labels the fluorophore brightness for the dynamic species i. There are 2 fitting parameters that one can extract from Eq. 3: First is the average concentration of particles sampling the observation volume, $\langle c_i\rangle$, which is inversely proportional to the amplitude $G(0)$. Second, the characteristic diffusion time, or the average time taken by the particle to transit the observation volume, $\tau_{D_i} = \omega_0^2/4D_i$ depends on the observation volume beam lateral waist radius, ω_0 and the diffusion coefficient of ith population (Fig 1A,B).

Similarly, if one assumes that particle concentration fluctuates purely due to the flow, then taking the second term of right-hand side

in Eq. 2 and solving the system of equations, followed by inserting the solution into Eq. 1 leads to a solution for ACF:

$$G(\tau) = \frac{1}{\pi\omega_0^2} \frac{\sum_{i=1}^{M} \langle c_i \rangle q_i^2 \times \exp\left(-\left(\frac{\tau}{\tau_{v_i}}\right)^2\right)}{\left(\sum_{i=1}^{M} \langle c_i \rangle q_i\right)^2} \tag{4}$$

As in Eq. 3, the amplitude relates to the average concentration of particles sampling the observation volume as they flow through. The characteristic time for $G(\tau)$ to decorrelate, $\tau_{v_i} = \omega_0/V_i$, which is defined as the average time taken by the particle to transit the observation volume, is linked to the observation volume lateral radius and to the speed V_i that *i*th species of particles use to sample the volume.

For the purpose of this article, we will not cover any other models and invite the readers to consult the literature for more details about the possible models (e.g., advection–diffusion and chemical reaction) and the solutions used for fitting the FCS ACF.

Now, we turn our attention to a natural extension of sampling the fluorescence fluctuation not only in time, as is case in FCS, but also in space. This was first implemented by ICS, where the idea of ergodicity was applied and the concept that in a stationary system, a temporal average is equivalent to spatial average of the ensemble. Therefore, in ICS, we correlate the fluctuation of fluorescence signal in pixel within an image, above and below average image intensity. The correlation function (CF) is computed over spatial lags rather than temporal lags as in FCS and gives rise to information, such as the average particle concentration per beam area (or per image). The original transition from FCS to ICS occurred with advent of modern LSCM, where the raster beam is scanned across sample and at each point of the sample fluorophores are excited for a time, depending on the scanner speed, and emit light that is then detected on a point detector, such as photomultiplier tube or avalanche photodiode. The effective observation volume in this scenario is a cross section (or convolution) between the scanning beam and the instrument point spread function (PSF) that is defined by the wavelength of the light used for imaging, as well as numeric aperture of the lens used for imaging. Later, ICS and different derived techniques were successfully applied to other imaging modalities, such as total internal reflection fluorescence microscopy that uses cameras (electron-multiplying charge-coupled device or scientific complementary metal-oxide semiconductor) to create the image. In that context, the observation volume is effectively the PSF of microscope. In other microscopy modalities, such as multiphoton excitation (2 photons, for instance), the excitation volume is very compact so that it effectively defines the observation volume. Independent of how an image or image time series is generated, we can write a general ICS CF, equivalent to $G(\tau)$ in FCS:

$$r_{ab}(\xi, \eta, \tau) = \frac{\langle \delta F_a(x,y,t) \delta F_b(x+\xi, y+\eta, t+\tau) \rangle}{\langle F_a(x,y,t) \rangle_t \langle F_b(x,y,t+\tau) \rangle_{t+\tau}} \tag{5}$$

where ξ, η, and τ denote lags in *x,y,* and time, respectively. Here, *a* and *b* denote the possibility of having 2 different imaging channels, representing potentially images of 2 proteins that interact in the system. For simplicity, we will consider only the single-channel imaging in this article but point the reader to the useful literature, later in section VII, where ICCS (and equivalently FCCS) are used to study protein colocalization and codynamics. In the current work, we present the fitting models of ICS for scenarios of ICS in context of single-image autocorrelation for extraction of particle number density within the single microscopy image, TICS for recovery of particle density and dynamical parameters, such as the diffusion coefficient and speed, and finally, STICS for recovery of particle flow from the image time series.

If we ignore the time component and correlate an image with itself ($a = b$), then Eq. 5, in analogy to development with Eqs. 1 and 2, but this time assuming no dynamics, the integral in Eq. 1 will be performed in space over a Gaussian excitation volume, leading to an expression of the ICS CF (see Appendix A for an example of derivation):

$$r(\xi,\eta) = \mathbf{r}(\mathbf{0},\mathbf{0})\exp\left\{-\frac{\xi^2+\eta^2}{\omega_0^2}\right\} + \mathbf{r}_\infty \quad (6)$$

In this case, the amplitude of the CF, $r(0, 0)$ is inversely proportional to the average number of particles that visit, by diffusion or flow, the observation volume of the imaging microscope; r_∞ is a fit parameter characterizing the offset of CF at infinity, usually equal to 0 if properly normalized (Fig 1C,D). If on the other hand, we correlate the intensity of each pixel with itself in time, ignoring the spatial lags, ξ and η, we obtain the equivalent of parallel FCS, but where each pixel from image time series is considered independently. This approach is known as TICS. In this case, depending of the underlying mechanism of particle movement and conversion (see Eq. 2), we will obtain different model functions for TICS fitting. For instance, if we have only diffusing particles, we will have the following model for fitting a TICS CF:

$$r(0,0,\tau) = \mathbf{r}(\mathbf{0},\mathbf{0},\mathbf{0})\left(1+\frac{\tau}{\tau_D}\right)^{-1} + \mathbf{r}_\infty \quad (7)$$

where the fitting parameter $\tau_D = \omega_0^2/4D$ is related to the diffusion coefficient and the observation volume lateral radius and r_∞ is defined in the same way as described previously. In the imaging sampling context, ω_0 is the lateral radius of the PSF. If the particles are purely flowing, the TICS CF will take the following form:

$$r(0,0,\tau) = \mathbf{r}(\mathbf{0},\mathbf{0},\mathbf{0})\exp\left(-\left(\frac{\tau}{\tau_f}\right)^2\right) + \mathbf{r}_\infty \quad (8)$$

where the characteristic time of CF decay is related to the particle speed in the following way: $v_f = \omega_0/\tau_f$. It is logical to see that if we have a system where 2 populations of particles coexist, where 1 diffuses purely and 1 flows with finite speed, we will have an expression for TICS CF that will be a sum of Eqs. 7 and 8, with amplitudes of each component inversely proportional to the particle species density (Fig 1E). Finally, if we consider the correlation of fluorescence fluctuations of every pixel in time series with every other pixel (i.e., applying the full spatiotemporal correlation as in Eq. 5), we will obtain STICS. The general expression for STICS CF will read

$$r(\xi,\eta,\tau) = \mathbf{r}(\mathbf{0},\mathbf{0},\tau)\exp\left\{-\frac{(\xi-\mathbf{x}(\tau))^2+(\eta-\mathbf{y}(\tau))^2}{\omega_\mathbf{0}^2(\tau)}\right\} + \mathbf{r}_\infty(\tau) \quad (9)$$

where $x(\tau)$ and $y(\tau)$ denote the x and y coordinates of the peak of the CF at lag time τ. Extracting the position of CF peak versus τ allows us to deduce the velocity of particles within the sampled field of view (FOV). Indeed, the slope of $x(\tau)$ versus τ gives the velocity along x direction, and a similar slope for the y coordinate gives the velocity along y axis (Fig 1F). On the other hand, if only diffusion is present, we do not expect the $x(\tau)$ and $y(\tau)$ to change over time. Therefore, this expression would reduce for single population diffusion to following expression:

$$r(\xi,\eta,\tau) = \mathbf{r}(\mathbf{0},\mathbf{0},\tau)\exp\left\{-\frac{\xi^2+\eta^2}{\omega_\mathbf{0}^2(\tau)}\right\} + \mathbf{r}_\infty(\tau) \quad (10)$$

and $\xi^2+\eta^2 = |\vec{r}|^2 = r^2$ is the radial spatial lag squared and the fitting parameter $\mathbf{r}(\mathbf{0}, \mathbf{0}, \tau)$ is inversely proportional to the number density of particles in the system. The other fitting parameter, $\omega_\mathbf{0}^2(\tau)$ can be written as

$$\omega_\mathbf{0}^2(\tau) = 4D\tau + \omega_0^2 \quad (11)$$

and ω_0 is the PSF lateral e^{-2} radius. This last expression is the equivalent of a mean square displacement (MSD), and STICS has been used in some contexts to characterize diffusion by using the CF radius squared ($\omega_0^2(\tau)$) change versus temporal lag τ.

III. PRELIMINARY CONSIDERATIONS

The Supplemental MATLAB scripts for the simulator and analyzer are provided in the Supplemental Material. Additionally, you can

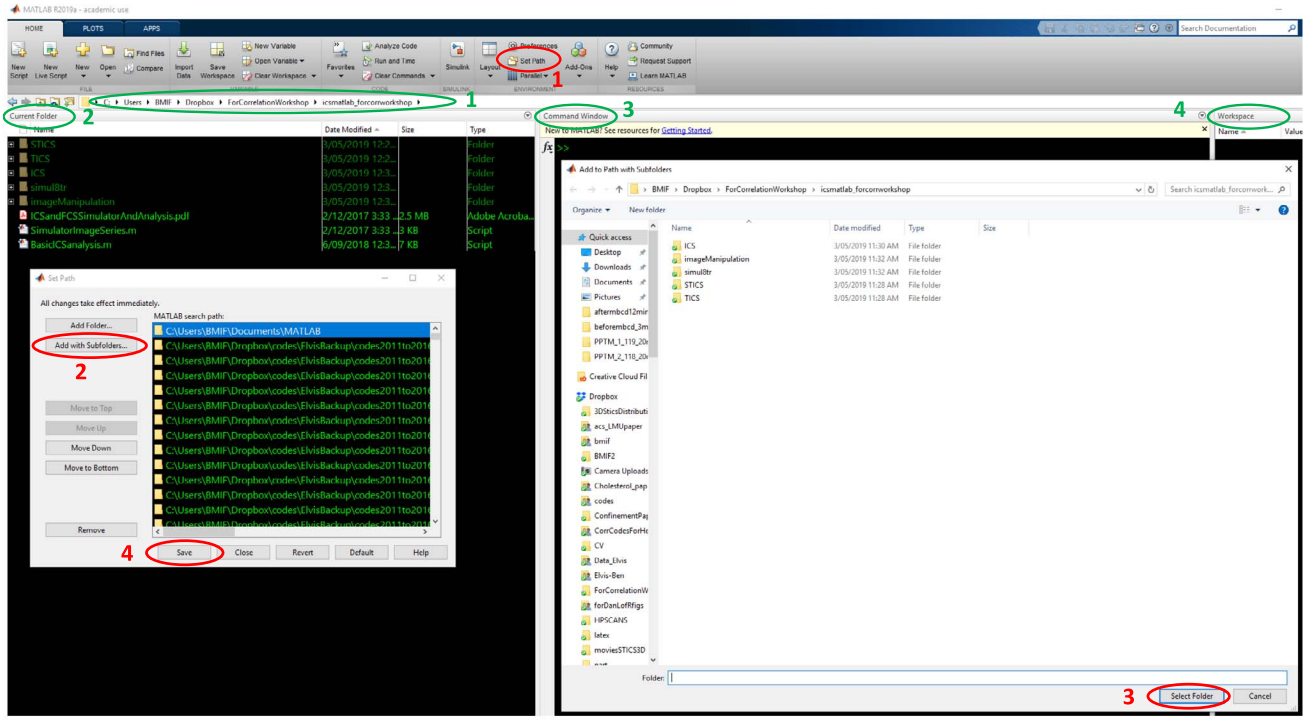

Fig 2. MATLAB interface. Setting the simulator and analysis scripts folder into the MATLAB path (red circles): (1) Set the path button used to open the dialogue with buttons (2) and (4); (2) add with subfolders button used to indicate the location of folder to be added to the path; (3) select folder is used to define main folder containing all the scripts and subfolders used in simulations and analysis.

find a copy of most up-to-date version of scripts at GitHub (https://github.com/ElvPan/Scripts-for-Biophysicist). To run the simulator and analysis scripts, the user will need to have MATLAB installed (preferably the latest version) with image processing, signal processing, and statistical toolboxes (see Appendix B for system requirements). For those that are unfamiliar with the MATLAB interface, we will start by introducing some essential parts and instruct how to add the scripts to the path. Please refer to the Figure 2 for details on how to add a folder with subfolders to the MATLAB path such that simulation and analysis scripts run properly. First, note that the current directory is displayed with green ellipse labeled as 1. Make sure that this is the directory of the folder containing your simulation and analysis scripts with subfolders as shown in green ellipse 2 and marked as the current folder. This is the directory you obtain after you extract the folder containing the scripts you will download with this article, named icsmatlab forcorrworkshop. Make sure you unzip the folder. Also, note that green ellipse 3 labels the command window, where the user can run lines of code or call execution of a script. Also, green ellipse 4 labels workspace, where the user can find all the variables generated throughout the simulations and analysis performed. To add the folder for simulation and analysis to MATLAB path, please click on set path as indicated by red ellipse 1 (Fig 2). It will open the dialogue prompting to select add with subfolders button, as shown in red ellipse 2. After this button is clicked, please select the main folder (red ellipse 3), containing all the subfolders and scripts used in this article (icsmatlab forcorrworkshop). Once you see that all the subfolders were added to the list of folders in the path, click on save, as shown in red ellipse 4. Now that the scripts are added to the MATLAB path, you are ready to proceed with simulating data and analyzing them by using one of the FFCS techniques. Enjoy simulating and analyzing!

IV. SIMULATOR

This section details the parameters that can be set by the user to simulate an image series, such as fluorescence microscope data or simulating the intensity fluctuation time series, as obtained in FCS experiments. The main function used for simulating datasets is SimulatorImageSeries.m, which can be found in the basic package inside the main folder icsmatlab forcorrworkshop. Beside the simulator script, this folder contains other subfolders containing scripts that can calculate basic modes of ICS or FCS and fit CFs, which will be detailed in later sections of this guide. To run the simulator, you will need to open a MATLAB session and open the script SimulatorImageSeries.m, followed by going to the editor tab of MATLAB and pressing the run button (or pause when activated). This action will open the simulator menu, as shown in the red circle in Figure 3 A. The user can set the following parameters in the simulator:

(a) Number of dynamical species: The default number of particle species is 1. In a complex cellular environment, more than 1 population of particles can sample an FOV, as will be demonstrated in few later examples.
(b) Image size in *x* and *y*: These 2 parameters define how big the images will be in pixels.
(c) Number of images: number of total images in the time series simulated.
(d) The pixelSize: the size of a pixel in micrometers.
(e) The timeFrame: the time delay between frames in seconds.
(f) PSF type: This defines if the PSF is Gaussian (g) or airy (a). For most of the wide field and confocal microscopes, observed PSF can be approximated by 3-dimensional (3D) Gaussian function, but the more exact function describing the emission profile is an airy function, hence, flexibility in choice.
(g) Lateral PSF e^{-2} radius (also known as ω_0): This specifies the radius of PSF, in micrometers, for the lateral (*xy*) plane.
(h) Axial PSF e^{-2} radius (also known as ω_z): This specifies the radius of PSF, in micrometers, for axial (*z*) plane. Leaving this at 0 ensures that particle dynamics occur in a 2-dimensional (2D) plane, such as the cell membrane, in which case the convolution with axial part of PSF is not necessary. Otherwise, the nonzero value needs to be entered if 3D dynamics are occurring (i.e. nonzero component of diffusion or flow in axial direction), but imaging still occurs in one plane. Also, set to the nonzero value if wanting to perform FCS simulations.
(i) Image bit depth: This specifies if output data is converted to 8, 10, 12, or 16 bits.
(j) Detector counting noise: This parameter (1 to 20) simulates the detector counting noise by using Poissonian-distributed noise (for image series simulations only).
(k) Background noise: This parameter (between 0 and 1) simulates the Gaussian background, where bigger values result in noisier data (for image series simulations only).
(l) Bleaching: This parameter specifies what kind of photophysics effect the user wants to impose on fluorophores. The default is none and implies no photophysics will be affecting fluorophores. Mono will result in monoexponential bleaching of fluorophores. Quantum dots (QD) will result in the power law blinking behavior of fluorophores, such as observed in QD.
(m) FCS: If the user wants to perform FCS simulation, then *y* should be entered. Otherwise, the default *n* will ensure image series with previously mentioned specifications is simulated. If the user decides to do FCS simulation, the answer here should be *y* and ensure that axial PSF e^{-2} radius is set to a nonzero value (usually $\sim$1 μm or 2 to 3 times the size of *xy* PSF radius).
(n) The mask size: This parameter, defaulted to 0 up until section VI.G, generates a central area mimicking cell, while the outside of the mask represents the space outside of a cell. If set to 0.5, it generates a square mask with edges half the size of full frame.

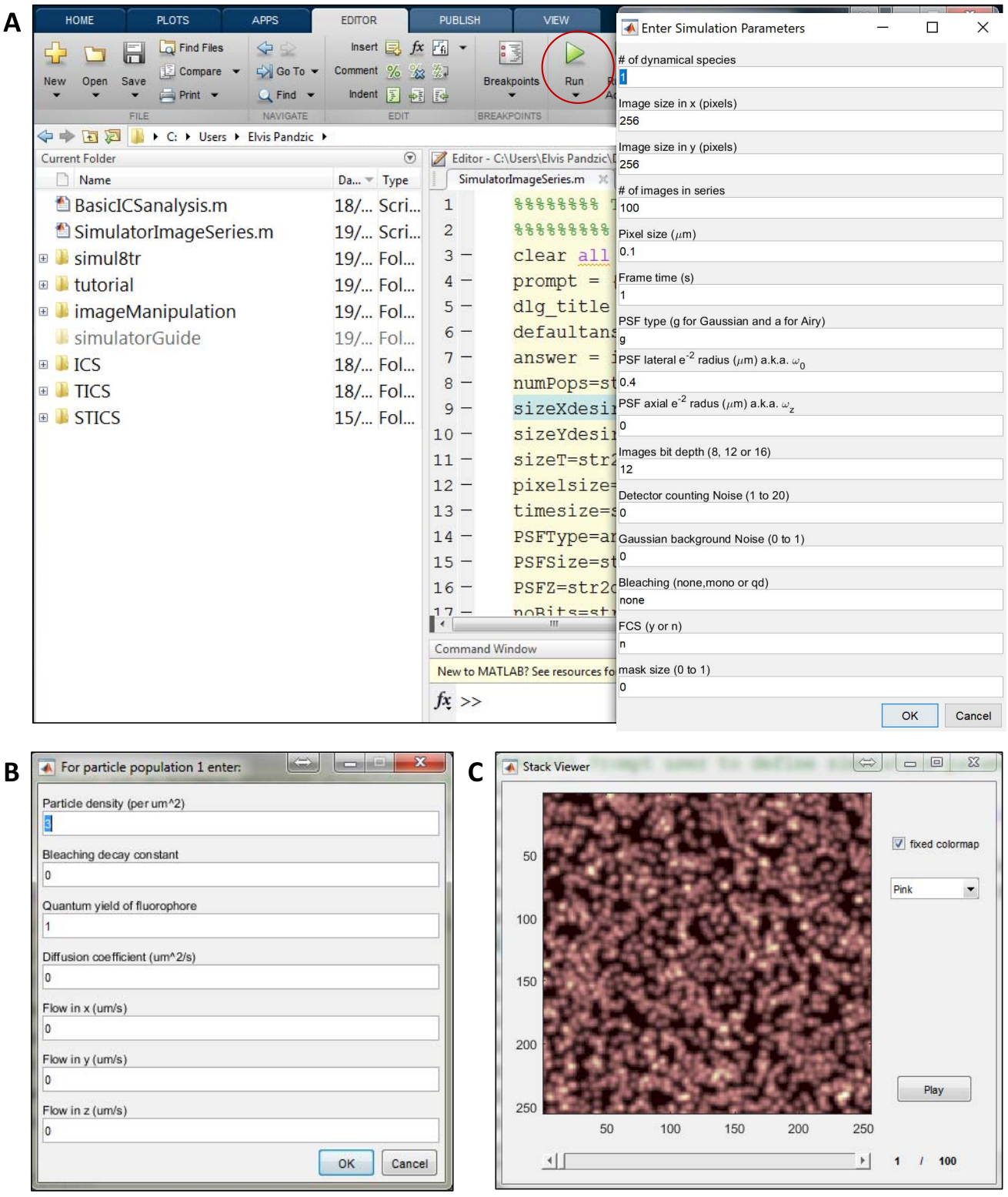

Fig 3. Simulator script. (A) User-defined input parameters for simulation to run. (B) Submenu for input parameters specific to each dynamic population simulated. (C) Example of simulated image series visualized by using the stack viewer (sv.m).

Once these input parameters are defined, the user can click on the OK button. This will open a new dialogue (Fig 3B), prompting the user to enter specific parameters for each particle population. If in the previous menu, the user entered several dynamical species to be simulated larger than 1, the same menu will open for every population. This submenu ensures that every dynamical population can be set to have different dynamics, quantum yield (brightness), and photophysics, such as the realistic scenario in which the same protein can be in several different cellular compartments and dynamical states.

The items in the submenu are the following:

(a) Particles density: defines the density of each particle population, in particles per micrometer squared.
(b) Bleaching decay: Depending on the bleaching value used in the previous menu, the bleaching decay numeric value will be the decay constant of the monoexponential bleaching. If on the other hand, the value in the previous menu was set to QD, the bleaching decay should be a 2-value array specifying the ON and OFF time exponents of the QD blinking distribution.
(c) Quantum yield (counts per pixel): This parameter specifies the quantum yield of a fluorophore. Default value is set to 1. If the user wants to simulate 1 of the populations as a tetramer, then input 4 at this parameter.
(d) Diffusion coefficient: parameter defining the diffusion coefficient of the population in micrometer per second.
(e) Flows X,Y and Z: These parameters define the components of flow of the population in the *x*, *y*, and *z* direction, respectively, in units of micrometer per second squared.

Once the simulation parameters are defined for all populations, the code will run and output a window showing the simulated data (Figure 3C). If an image time series was simulated, the series viewer (sv) can be used to play the image time series. Once visualized, sv can be closed, and you can proceed with analysis as outlined in the following sections.

V. FCS simulations and analysis

This section shows how the simulator can be used to generate an intensity time sequence similar to the one obtained in FCS experiments. This simulator does not explicitly consider more complex scenarios in FCS experiments, where the various fluorophores' photokinetics are involved, nor does it allow for realistic control of detector gain and other detection parameters. Nevertheless, it allows the user to perform some basic FCS simulation and to appreciate how the variability in particle population density and dynamics parameters can affect the ACF in FCS. To generate a FCS sequence, run the SimulatorImageSeries.m script and make sure to input a nonzero value of PSF axial radius (usually 1 to 1.5 μm), the FCS field to y and number of images in series to 10,000 at least (see Fig 3). Once the user clicks the OK button, a menu will pop up for each population of particles, as shown in Figure 3B. Choose the values you want to simulate for each population. After the simulator has generated a sequence, it will produce a plot of intensities versus time as shown in Figure 4A. Feel free to use the zoom in tool on MATLAB figure window to zoom in intensity sequence and see how the intensity fluctuations differ with varying simulation input parameters (Fig 4B).

A. Running FCS or ICS analysis

To perform FCS or ICS analysis, run BasicICSAnalysis.m inside icsmatlab forcorrworkshop matlab folder by clicking on run (shown as pause in Fig 5A) button. This will open the dialogue, as shown in Figure 5A.

(a) ICS for $\langle N \rangle$: Run spatial ICS analysis on single images (used to extract the number density of particles).
(b) TICS for speed and diffusion: Run temporal fluctuation correlation in single pixels of image time series (used to extract number densities, diffusion coefficient, or speed of particles).
(c) STICS for flow: Run spatiotemporal correlation on full time series for flow analysis.
(d) The FCS: used to extract parameters, such as number densities, diffusion coefficients,

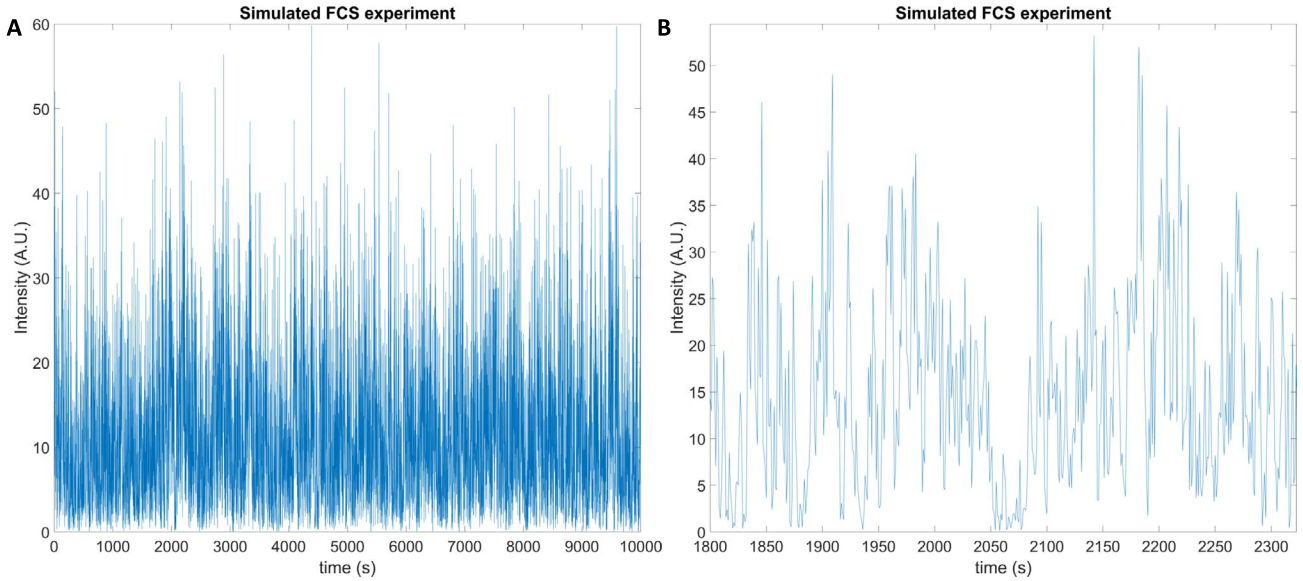

Fig 4. The intensity sequence output of FCS simulation. The data was generated using $D = 0.03$ μm^2 s^{-1}, density = 1.5 particles per micrometer squared, and axial PSF radius of 1.2 μm.

and speed of particles from FCS experiments.

B. FCS simulation case 1: free diffusion in 3D

FCS data simulated and shown in Figure 4 was produced by using $D = 0.03$ μm^2 s^{-1}, density = 1.5 particles μm^{-2}, and axial PSF radius of 1.2 μm. To perform FCS analysis, open the script BasicICSAnalysis.m. It will open the menu dialogue, prompting the user to select one of the analysis methods, as shown in Figure 5A. Selecting FCS and pressing the close button will run the calculation of FCS ACF. The calculated ACF is plotted (Fig 5B), and a new menu will appear, prompting the user to select the fitting model (Fig 5C). The fitting model choices are the following:

(a) The 1 component diffusion: This model assumes that data is sampled from a single freely diffusing particle population. It assumes that motion happens in 2D.
(b) The 1 component flow: This model assumes that data is sampled from a single actively transported particle population. It assumes that motion happens in 2D.
(c) Sum of 1 component diffusing and 1 component flowing: This model assumes that data is sampled from a 2 independent particle population, 1 actively transported and 1 diffusing. It assumes that motion happens in 2D.
(d) Single component 3D diffusion: This model assumes that data was collected from a sample containing 1 dominant diffusing population in 3D.

For the simulated FCS data in Figure 4, we selected 1 component diffusion and ran it by pressing the close button. A new window (Fig 5D) will appear, prompting the user to enter some of the microscope related parameters, which can either be coming from simulated data (as in the case considered) or from real experimental data. Make sure to enter the correct values, such as radial and axial PSF radii and sampling time used in simulation, as well as determine the maximum temporal lag for which the ACF should be calculated, usually about a 10th of the total experiment time, and press OK.

We will use the Eq. 3 here to fit the FCS ACF. The fitted results will be displayed as in Figure 6, with raw data displayed and fit (red line) superimposed. Also, residuals of the fit are shown for a visual inspection of the goodness of fit and to help the user determine if the model used fit the data well. Moreover, the user

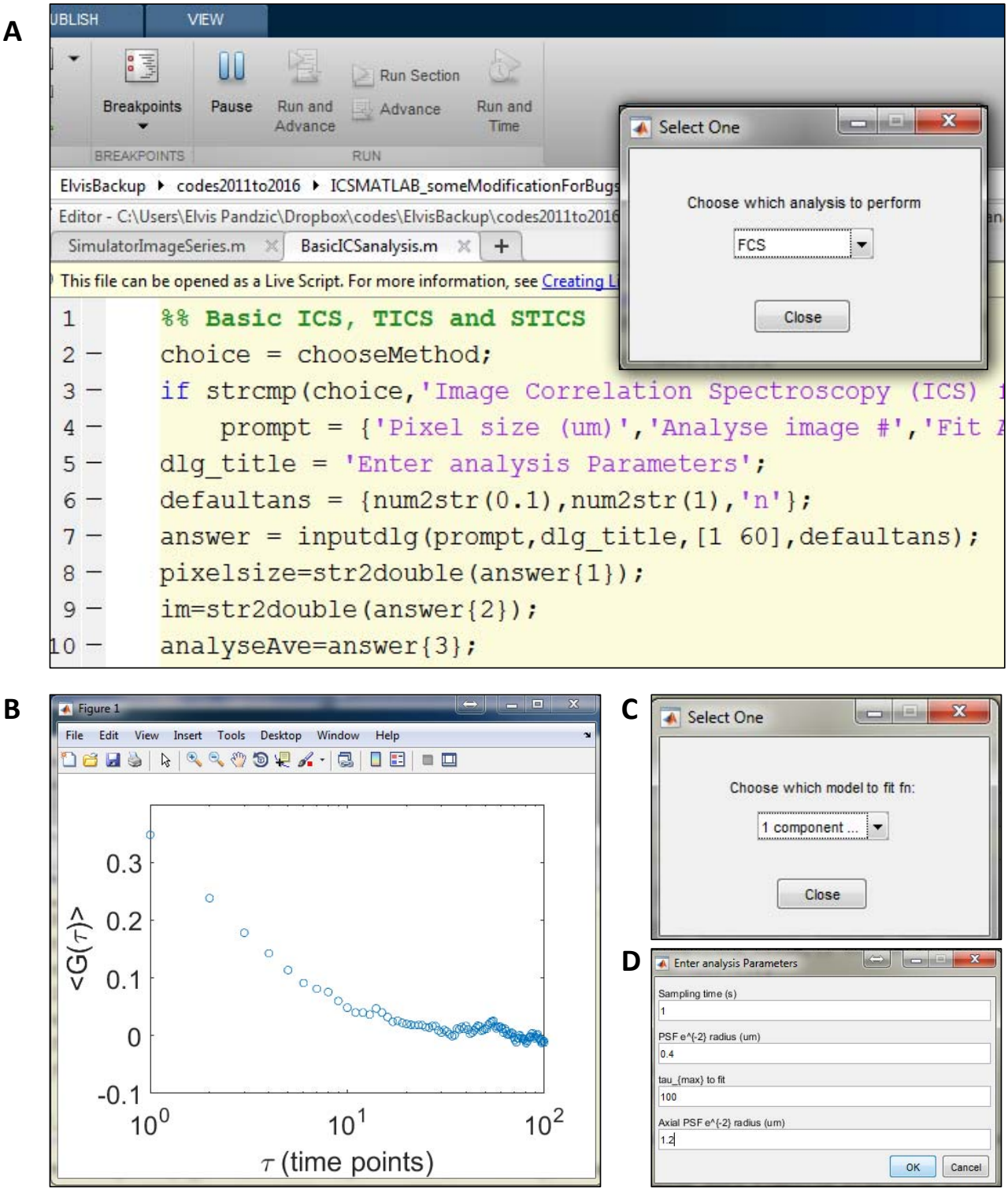

Fig 5. The user prompt for analysis of FCS or ICS series. (A) Prompt dialogue for analysis. (B) Example of FCS ACF from the simulated example in Figure 4. (C) Prompt for choice of ACF fitting method. (D) Prompt for FCS analysis input parameters.

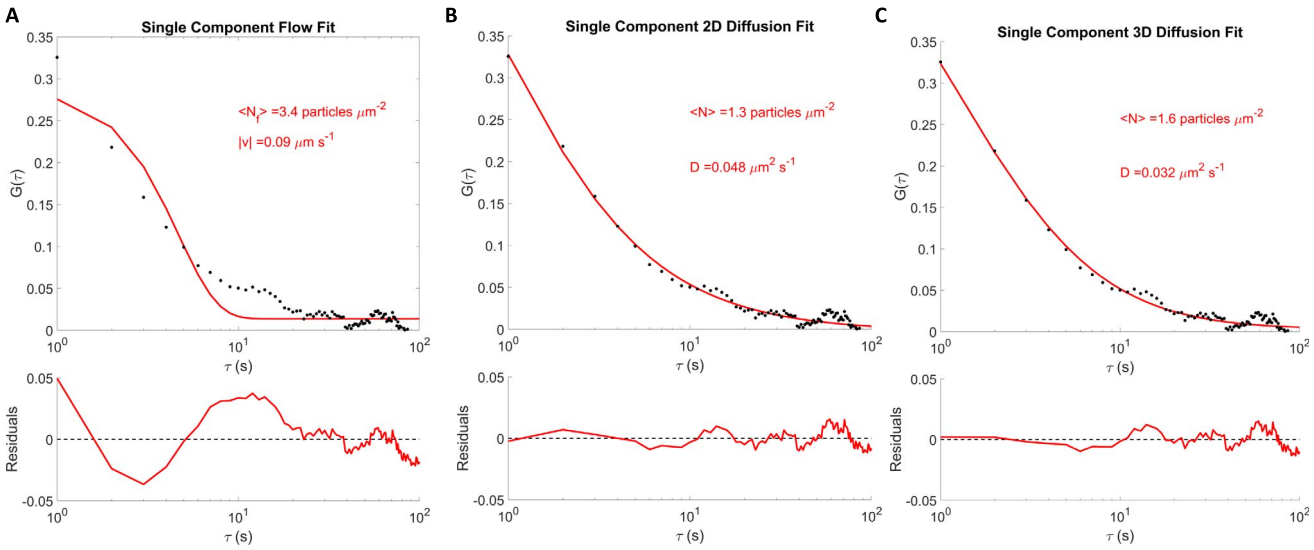

Fig 6. Fitting 3D diffusion simulated FCS data ACF with 3 different models. (A) Fitting single-component flow model, (B) fitting 2D diffusion model, and (C) fitting 3D diffusion model.

will be able to see the number density $\langle N \rangle$ and diffusion coefficient recovered from the fitted parameters (values displayed in red to the right of fitted curve).

Q1 for the learner

According to your observation from the 2D diffusion fit model (Fig 6B), does this model provide a good fit the ACF? Does it recover the set simulation parameters for $\langle N \rangle$ and D? Now, rerunning BasicICSAnalysis.m, with FCS mode and select the single component 3D diffusion as a fitting model, should produce the graph as shown in Figure 6C. Are recovered parameters of $\langle N \rangle$ and D closer to the set simulation values? Try fitting the other available fitting models for FCS and see how they compare. Can you think of other metrics to assess the goodness of fit and, ultimately, verify which model best fits your data?

See Appendix C for the answers and discussion.

C. FCS simulation case 2: 1 flowing population

For this exercise, we simulate FCS data with particles flowing in 3D. Make sure to run SimulatorImageSeries.m and select FCS to simulate FCS data and input simulation parameters as in previous example, but this time input flow values as shown in Figure 7A.

Run BasicICSAnalysis.m and try fitting 1 component diffusion in the 2D model (see Eq. 4). It will produce a graph as shown in Figure 7B.

Q2 for the learner

Does the model fit the data well? How about the recovered parameters? Now, try fitting 1 component flow model. It should produce the plot in Figure 7C. Which model fits ACF best and why? How do recovered values for flow speed and particle number density compare to the values set in FCS simulation?

D. FCS simulation case 3: 1 component diffusing and 1 flowing

Repeat the simulation steps from previous sections (Fig 8A), but this time, select 2 dynamical populations. For a variation, change the time step from 1 to 0.1 s and simulate 50,000 steps rather than 10,000. Ensure that you adjust the axial PSF radius and input y at the FCS input. Adjust densities and dynamic parameters of diffusing and flowing populations, as shown in Figure 8B,C. Once the FCS data is simulated and intensity trace graph like the one shown in Figure 4, is generated, close it and run BasicICSAnalysis.m, with the FCS mode. The ACF will pop up with input dialogue for selection of the fitting model, as shown in Figure 8D. Select sum of 1 component diffusing

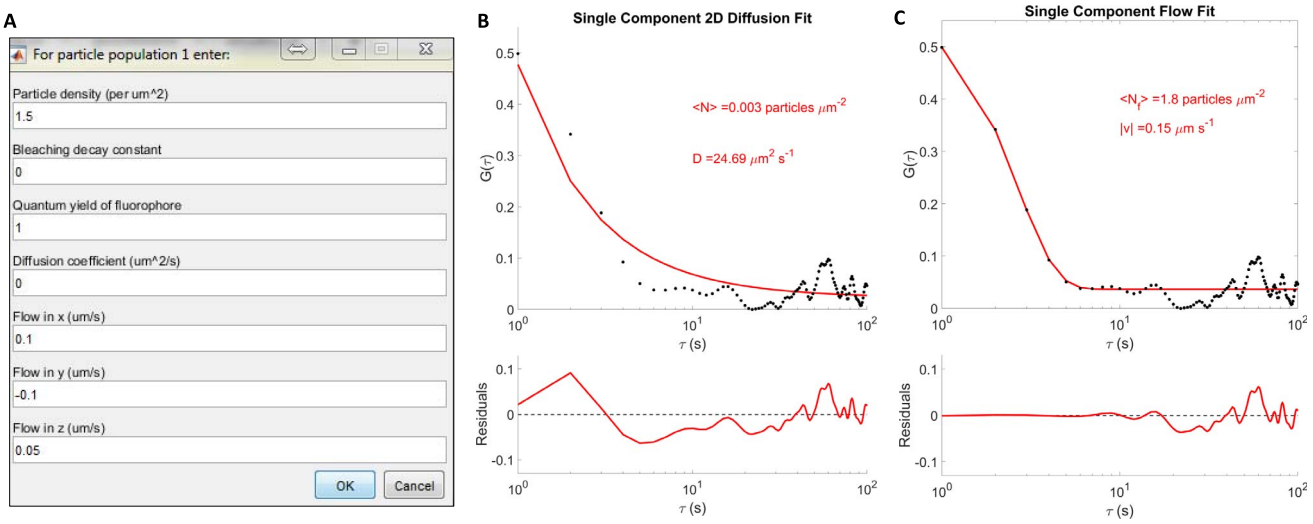

Fig 7. Simulating 3D particle flow FCS data and calculating and fitting ACF with 2 different models. (A) Inputs for FCS simulation of flow. (B) The 2D diffusion model fit. (C) The 3D flow model fit.

and 1 component flowing for fitting model (combination of Eqs. 3 and 4) and click on the close button (Fig 8D inset). This will generate the fitted results, as shown in Figure 8E.

Q3 for the learner

Do the fitted results make sense compared with set inputs for simulations? What if you tried different fitting models presented in previous sections? Moreover, how would you set up the simulation to see decays from 3 populations, say 2 diffusing and 1 flowing. What should be total time of acquisition? Considering their respective average transit time through the PSF and the PSF size you would use, what should be the total number of time points of acquisition?

VI. ICS SIMULATIONS AND ANALYSIS

In the first section, we saw how to generate a time series by using SimulatorImageSeries.m script. Using the same simulation settings as detailed in Figure 3A,B, generate the image series, shown in Figure 3C. This simulation generates an immobile population. Open the BasicICSAnalysis.m script and run it, selecting the ICS for $\langle N \rangle$ to run ICS analysis. It will pop open a menu, as shown in Figure 9A, prompting the user to enter the pixel size (in micrometers) of which image of the series to analyze, if the average ICS CF should be fitted instead of single image CF, and if the (0,0) spatial lag should be ignored in fitting. In the following examples, a few cases of ICS simulations are explored.

A. ICS simulation case 1: ICS for recovery of $\langle N \rangle$

With parameters set as in Figure 3A,B, generate an image time series. In the analysis menu for ICS, enter values, as shown in Figure 9A. In this case, we fit the ICS ACF with Eq. 6 and use the amplitude to extract $\langle N \rangle$. Considering that the simulation used 3 particles per micrometer squared and the PSF lateral radius of 0.4 μm (area of ~0.5 μm^2), how do recovered values compare with input? Now try the same analysis, but this time enter y in the menu, next to the fit average. You will likely not see any difference because the population is immobile; hence, all the images in the time series are identical. Therefore, the average ACF from ICS will be identical to the ACF from a single image. Try simulating a time series where you add some motion to the particles such as diffusion. Repeat the ICS analysis but on a single plane ACF. You should have results similar to the one shown in Figure 9D.

Q4 for the learner

What if now you rerun the ICS analysis on the same dataset, but this time, choose to take the temporal average of the ICS ACF and fit it with

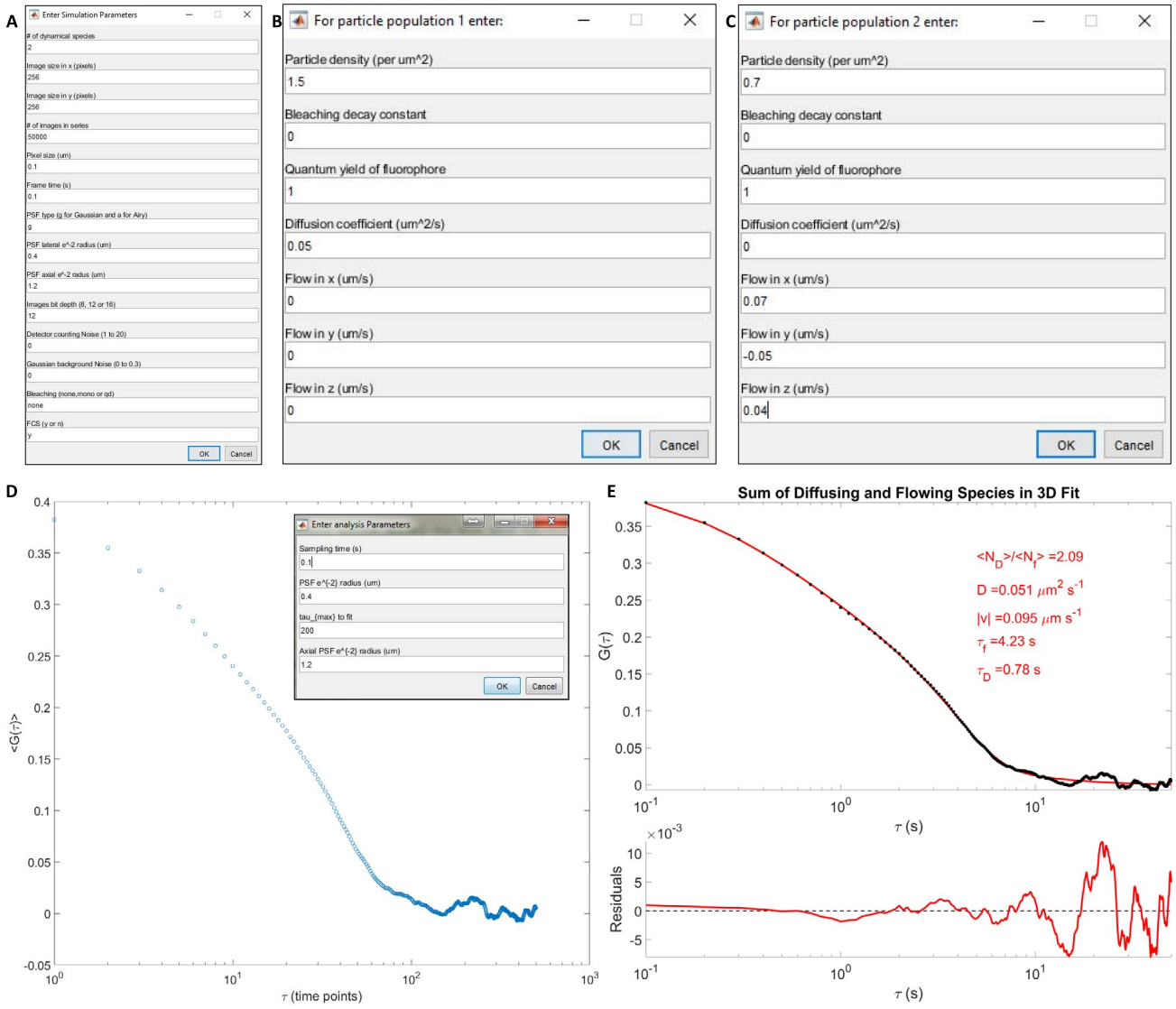

Fig 8. (A) Input dialogues for simulating a diffusing and a flowing population in FCS experiment. (B) Input parameters for diffusing population. (C) Input parameters for flowing population. (D) ACF for simulated sum of flow and diffusion. Inset: input parameters for fitting model. (E) Results of fitting sum of flow and diffusion components.

the 2D Gaussian (Fig 9E). Will the fit improve compared with the fit of an ACF from a single image plane (Fig 9F). Any improvement in output values for the density of particles compared with the set values in simulation?

B. ICS simulation case 2: TICS for recovery of particles diffusion coefficient

In this section, we explore how to use TICS (i.e., temporal correlation of individual pixels in a time series) to recover dynamics of particles. Generate image time series by using settings as shown in Figure 3A,B, but set diffusion coefficient and density of the populations to $D = 0.01$ μm^2 s^{-1} and 3 particles per micrometer squared, respectively. Run BasicICSAnalysis.m, selecting TICS for speed and diffusion, as shown in Figure 10A. This is similar to running FCS analysis on intensity sequence, as detailed in section V, case 1, but here, each pixel's intensity of the image series fluctuates due to underlying particle movement. TICS is a bit of a parallelized FCS for slow dynamics, as captured on imaging frame rates.

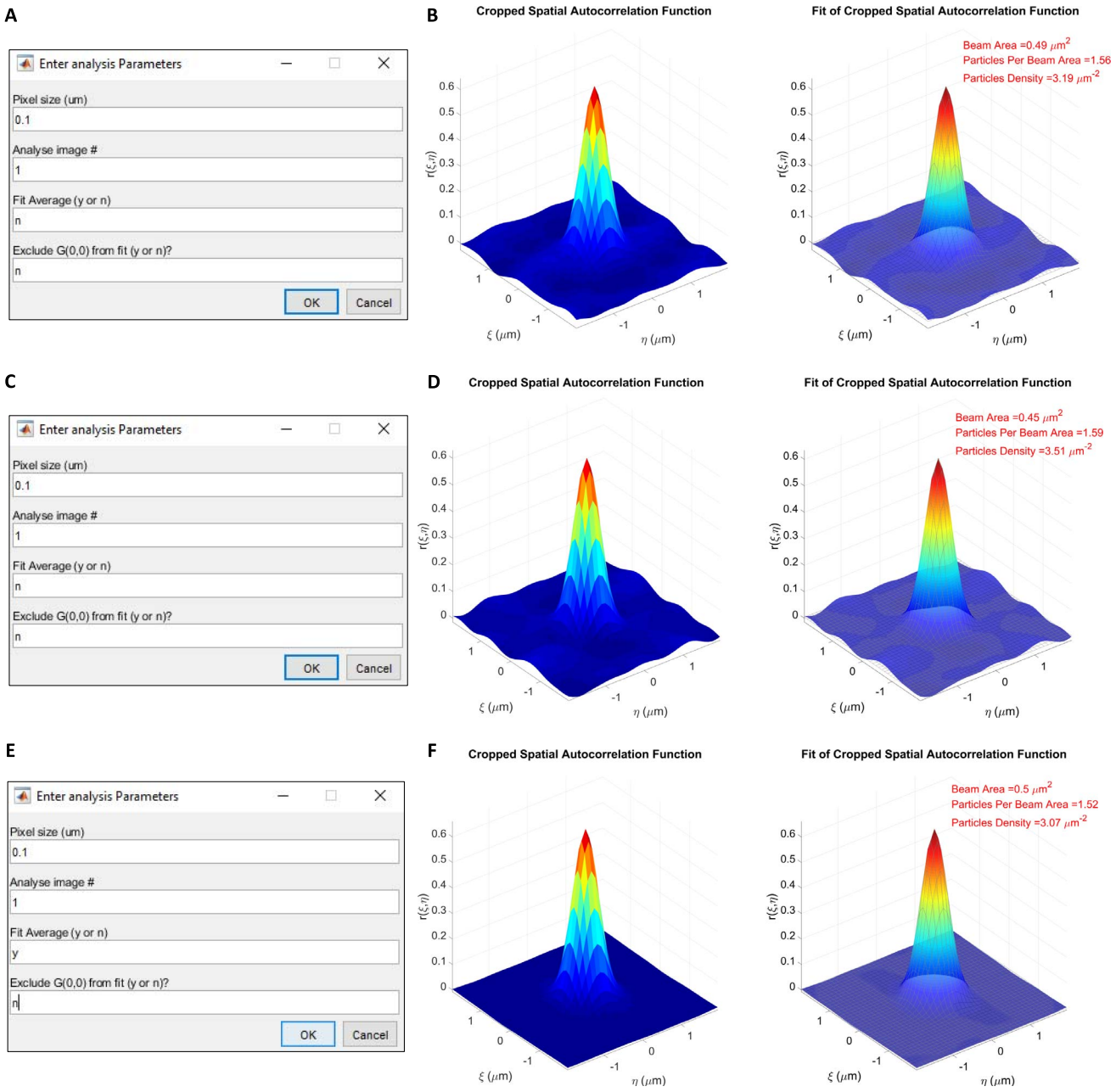

Fig 9. ICS analysis for recovery of number density of particles. (A) ICS input dialog for analyzing a single image from an image series of immobile particle population. (B) Raw and fitted CF from ICS analysis for a single frame of a simulated immobile particle population. (C) ICS input dialog for analyzing a single image from an image series of freely diffusing particle population. (D) Raw and fitted CF from ICS analysis for a single frame of a simulated freely diffusing particle population. (E) ICS input dialog for analyzing the temporal average of the ICS ACF from an image series of diffusing particle population. (F) Raw and fitted ACF from ICS analysis for the temporal average of the ICS ACF from an image series of simulated diffusing particle population.

The TICS analysis will be applied to the image time series, and a spatial pixel average CF will be displayed on the screen, as shown in Figure 10B. Moreover, a dialogue menu will open, prompting the user to pick a model to fit the CF (see Eq. 7). Select 1 component diffusion and press the close button to proceed. Another menu will open prompting for frame time(s), radial and axial e^{-2} radii of PSF, and maximum temporal lag (τ) to be considered in fitting. Make sure that input parameters reflect what you used to simulate the data, or in case of experimental data use, the acquisition parameters used to acquire image series. For now,

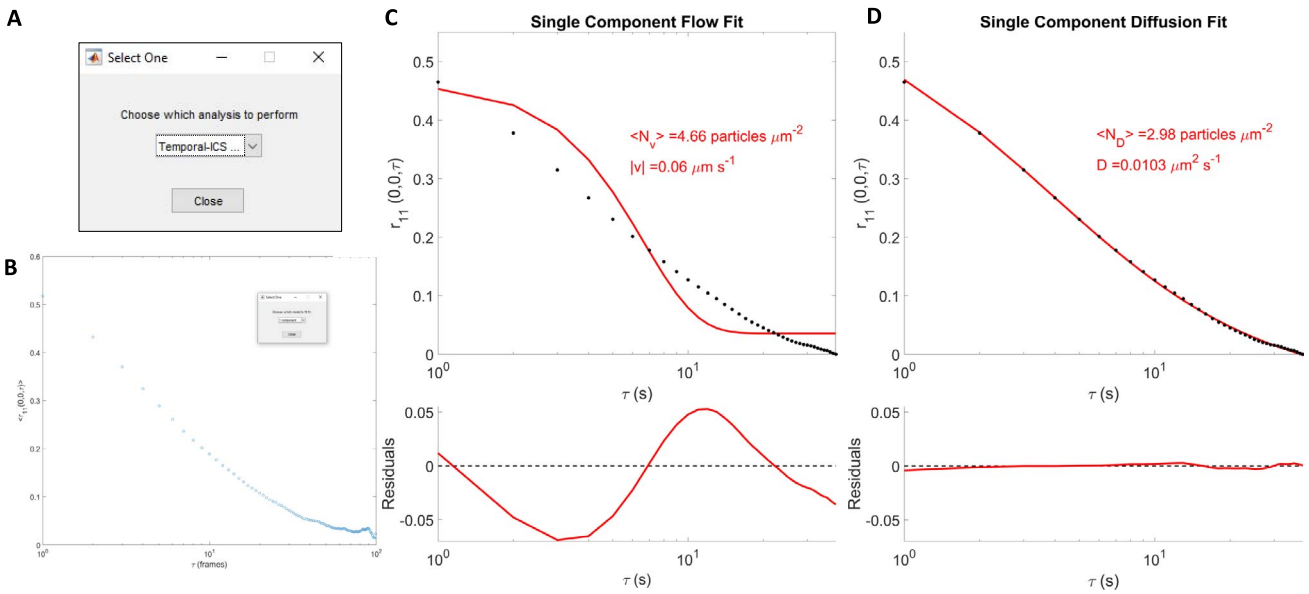

Fig 10. Running TICS menu from BasicICSAnalysis.m to analyze simulated image time series. (A) Select TICS from prompt dialogue for analysis and (B) TICS ACF function and prompt for fitting model. (C) Fitting results for flow model fitted on the TICS ACF for the free diffusion simulated data. (D) Fitting results for diffusion model fitted on the TICS ACF for the free diffusion simulated data.

you can ignore (set to 0) axial radius of PSF, as we simulated the 2D diffusion in this example. Click OK, and it will proceed with TICS analysis and fitting. Figure 10D shows results of fitting a single 2D diffusion model to the TICS CF.

Q5 for the learner

Do the recovered parameters compare with set density of particles and diffusion coefficient? Try running the TICS analysis again, but this time, select 1 component flow. It should produce the plot, as in Figure 10C. Compare results.

C. ICS simulation case 3: TICS for recovery of particles speed

In this section, we run the SimulatorImageSeries.m to generate the flowing particles image series. After the first menu, as shown in Figure 3A, you will be prompted to enter the particle population specific parameters, as shown in Figure 11A.

Try fitting a free diffusion model to the data (Fig 11C). Does it fit well the data? Fitting the 2D flow model (see Eq. 8) for TICS leads to a more accurate estimate of parameters used to simulate the data (Fig 11D). More importantly, this model fits more accurately the ACF.

D. ICS simulation case 4: STICS for recovery of particles flow

As already demonstrated, TICS analysis can recover the speed of flowing particles within a considered region of interest but cannot distinguish in which direction flow occurs. Full STICS can be used to pick both magnitude and direction of flow. Rerun the analysis script on data simulated in previous section, but this time, select STICS for flow when prompted in the analysis menu (Fig 12A). This will open a menu for STICS (Fig 12B) input parameters. For now, leave the immobile filtering parameter at n, as we do not have any immobile particles in the image series simulated. Run the code by clicking OK. The fitting model used here is described by Eq. 9.

This will open the window containing the STICS CF that can be played (stack viewer). Please wait until the STICS CF fitting is complete and results are displayed, as shown in Figure 12F. The STICS CF peak (Fig 12C–E) translates at the same rate as the molecules simulated in the time series. Detecting the peak of CF at every temporal lag τ and fitting the position in both x and y directions versus τ leads to full flow information (v_x,v_y).

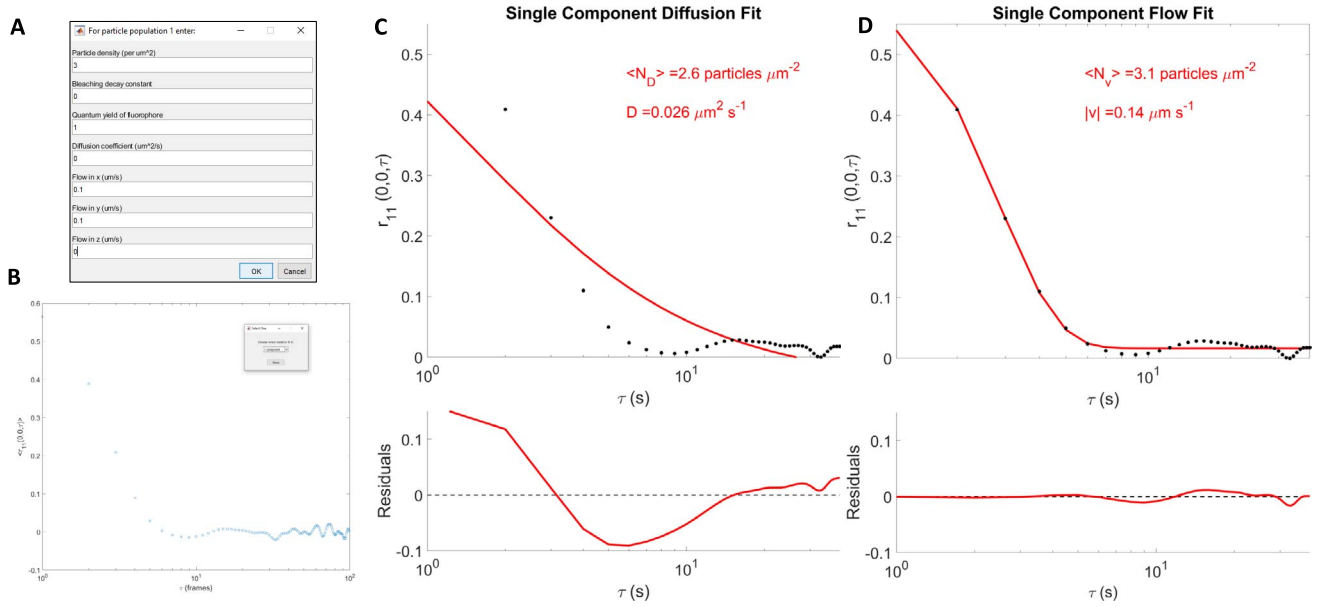

Fig 11. The 2D flow image series simulation and TICS analysis. (A) Input parameters for 2D flow simulation. (B) TICS ACF for simulated 2D flow image series and prompt for fitting model (inset). (C) Single component diffusion fitted to TICS ACF of simulated 2D flow population. (D) Single component flow fitted to TICS ACF of simulated 2D flow population time series.

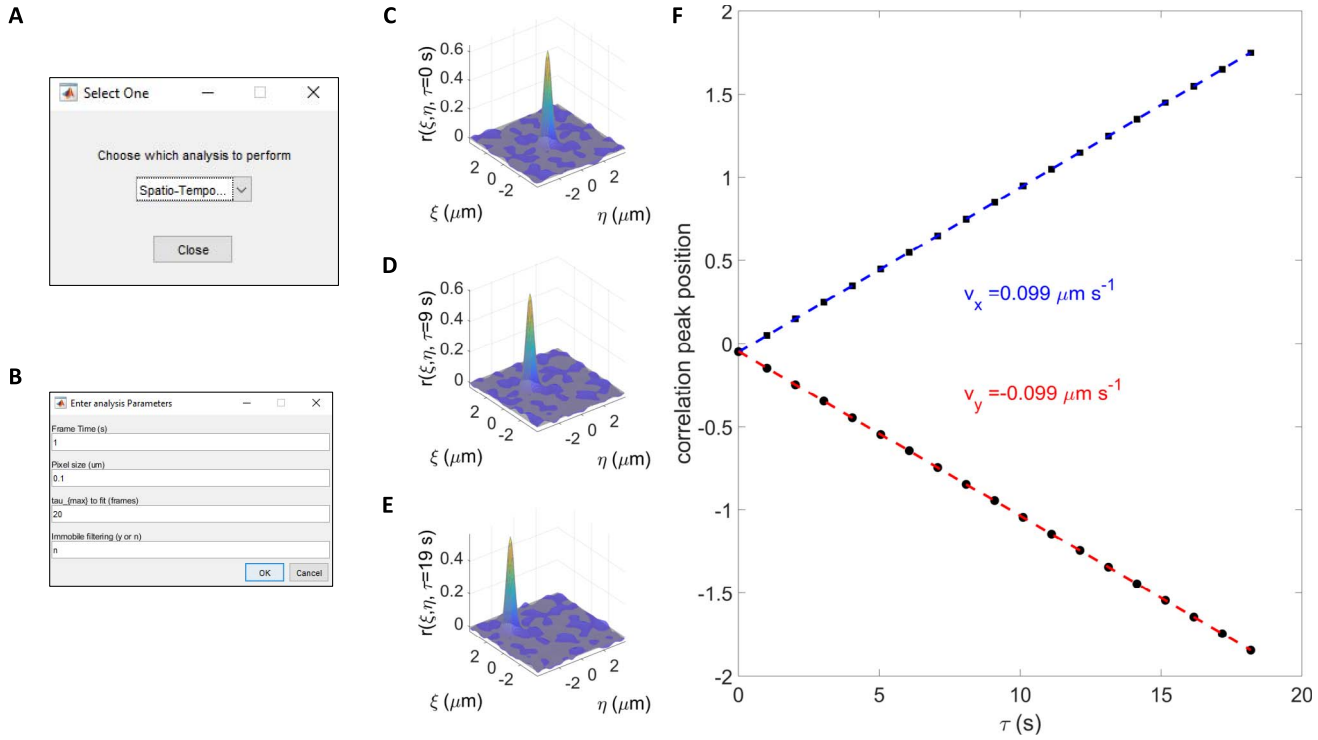

Fig 12. Input prompt for choice of analysis method, STICS input parameters, and results from STICS analysis of simulated flow example. (A) Prompt for selecting analysis method. (B) STICS input dialog. (C), (D), and (E) STICS CF for temporal lags $\tau = 0$, 9, and 19 s. (F) Extracting the position of CF peak at different temporal lags, τ and fitting linearly versus τ allows for recovery of velocities (slopes of fit) along both *x* and *y* directions.

Q6 for the learner

Do the values recovered compare with the set parameters in the simulation? If you had multiple populations flowing, what do you expect STICS CF to look like?

E. ICS simulation case 5: STICS for recovery of particles flow in presence of immobile particle population

Rerun the simulation of image series, but in this scenario, use 2 particle populations and specifications, as shown in Figure 13A. When prompted to input parameters for each population, make the first population flow a defined amount, as in Figure 13B, while making the second population immobile (Fig 13C). This will generate STICS analysis results as shown in Figure 13F. Obviously, extracted flow is biased because the immobile population peak at the origin of CF (Fig 13F) affects the fitting and recovery of the flowing peak. To remedy this problem, we can filter the immobile contribution from the image time series by applying the immobile filter. It can be done by subtracting the temporal average image of the time series from each frame or by taking the temporal Fourier transform of the time series and setting the lowest (slowest) spectral component amplitude to zero, with Fourier inverting the resulting time sequence. If we apply the immobile filter in this way, by setting immobile filtering parameter at y in the menu shown in Figure 13E, we will remove the immobile population from time series and effectively recover the right flow from STICS analysis of the immobile filtered image series, as shown in Figure 13G.

F. ICS simulation case 6: STICS for recovery of particles flow for simultaneously flowing and diffusing particles

Set up another simulation where you simulate a single population of particles by using settings shown in Figure 14A. When prompted to define the dynamic properties of the particle population, enter values of diffusion and flow, as shown in Figure 14B. This will generate a time series in which particles simultaneously flow and diffuse. Perform STICS analysis (Fig 14C) and examine the results (Fig 14D).

Q7 for the learner

What are characteristics of the STICS CF in this case? Did the linear fit of the CF position versus τ produce accurate estimate of flow in both the x and y directions? What happens with CF width as τ increases? Can you think how would this information be useful? What dynamic parameter would we be able to recover from it?

G. ICS simulation case 7: number density recovery in the presence of background noise

In this section, we simulate data that represents common experimental scenarios, such as the one in which background noise is present in the image data. The noise in the data can originate from different components of samples, such as the autofluorescence from the cell culture medium, cells aromatic residues, and nonspecific binding of dyes to the culture dish coverslips. Even the instrument components such as dirty filters or other optical components can give rise to noise. More commonly, detectors being electronic devices that generate heat and with it, a significant amount of background, called Gaussian noise, which may be detected in the image. This noise is normally distributed and additive in nature. There are other types of noises, such as salt-and-pepper noise, which originates from analog-to-digital image conversion and can be somewhat corrected by median filtering. Finally, the inherent nature of statistical quantum fluctuations and variability in emitted photons from different parts of sample will result in so-called shot noise. This noise is characterized by being proportional to the square root of the image intensity and, as such, is Poissonian in nature. Shot noise is embedded in simulation parameter called counting noise.

Herein, we simulate the effect of background or Gaussian noise and demonstrate how it can be corrected in ICS analysis. Please proceed with simulation, as shown in Fig 15A, which is basically the same as section VI.B, except this

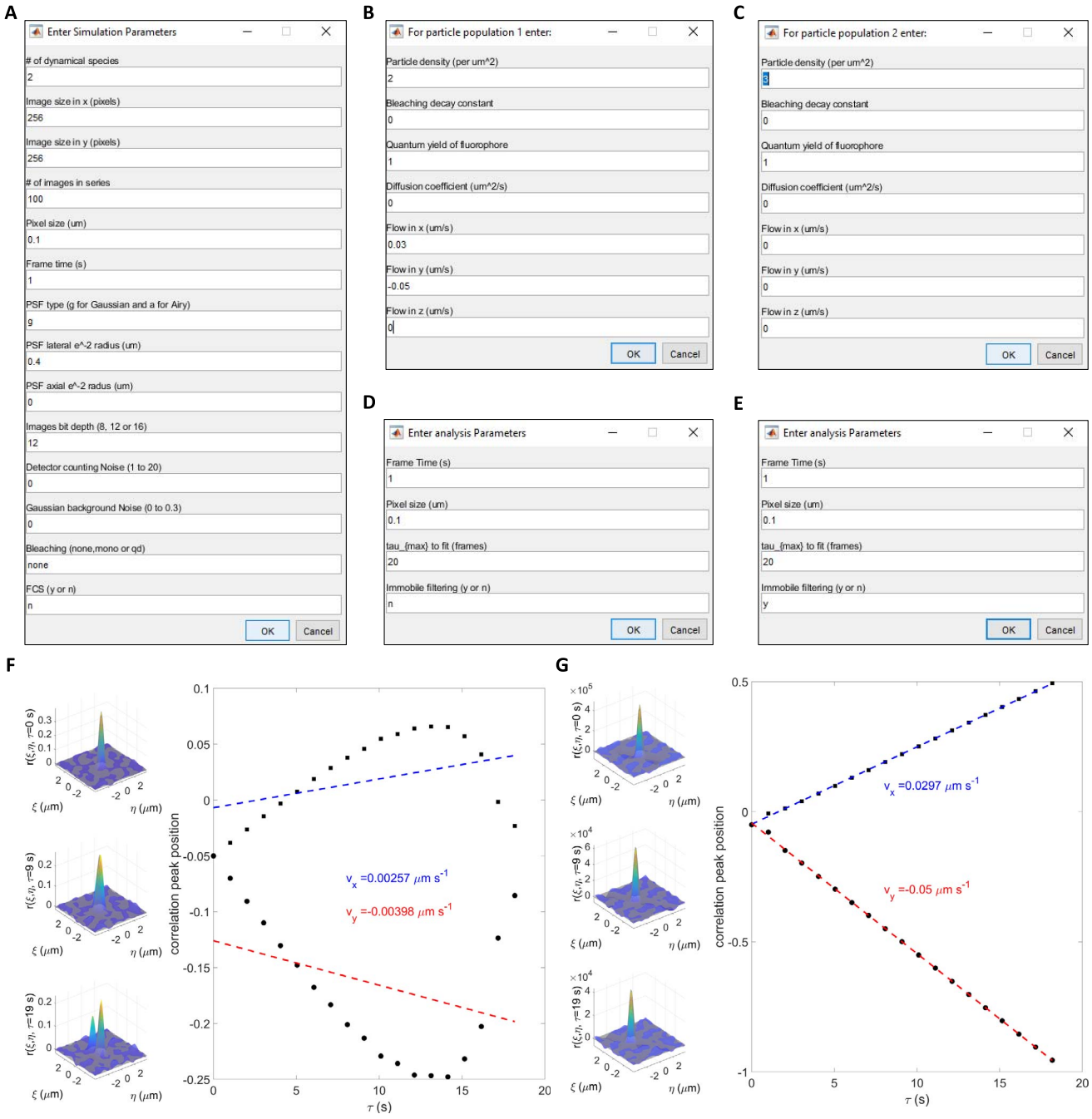

Fig 13. Input dialogues for simulating 2 flowing populations in ICS experiment. (A) Inputs for image series simulation of 2 flowing populations. (B) Input parameters for flow population 1. (C) Input parameters for flow population 2. (D) Prompts and (F) results for STICS analysis of a flowing and an immobile particle population simulated data. (E) Prompts and (G) results for STICS analysis of a flowing and an immobile particle population simulated data and postimmobile filtering of image series.

time, change the "Gaussian background noise" parameter to 0.2. At this point, leave "mask size" parameter at 0. When prompted for dynamical parameters, just change the diffusion coefficient to 0.01 $\mu m^2\ s^{-1}$, as in section VI.B. This will generate an image time series that will be opened in the stack viewer, shown in Figure 15D. As you can observe, having the Gaussian background noise set at 0.2 produces a noisy time series with a signal-to-noise ratio of $1/0.2 = 5$. At that signal-to-noise ratio, we can still perceive the particle movement. Apply ICS as shown in the prompt in Figure 15B. The data is shown in Figure 15E. The raw CF (left)

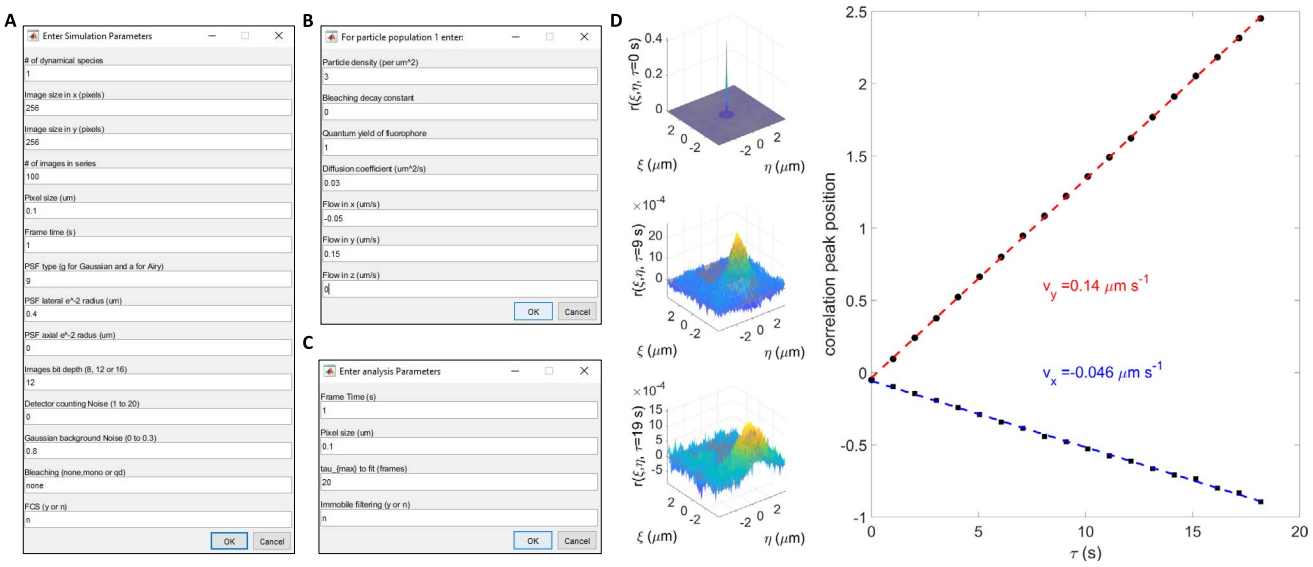

Fig 14. Input dialogues for simulating simultaneously flowing and diffusing population in ICS experiment. (A) Inputs for image series simulation. (B) Input parameters for particles dynamics specifications 1. (C) Prompts and (D) results for STICS analysis of a simultaneously flowing and diffusing particle population simulated data.

has a spike at $G(0,0)$ superimposed on a regular Gaussian-like ICS peak. This is a signature of noise in image data and how it affects ICS CF. Because noise does not correlate over larger than single pixel distance, the larger than (0,0) spatial lag will be less affected by noise. When the average CF is fitted, but including the $G(0,0)$ value, we clearly do not have a good fit as shown in center panel of Figure 15E. The recovered value of particle density 15 per micrometer squared is 5 times the set value. If on the other hand. we rerun analysis, but this time, select to exclude $G(0,0)$ in fitting (Fig 15C), we obtain better fit to ICS CF, as shown in Figure 15E on the right panel. Still, the recovered value of number density is far from set value. The problem here is that our data is corrupted with Gaussian noise. The simulated images (Fig 15D) would be the equivalent of imaging a square area inside a cell surface. This way, we do not have an external to the cell area reference of how bad the Background noise is.

If we resimulate data, setting the mask size parameter to 0.5 as in Figure 15A, it will produce the dataset similar to the one shown in Figure 15F. In this case, we generated a celllike area mimicked by an inner square and an outer area that simulates outside of the cell area. In this data, it is now clear how much background noise adds to the images, even in the parts of the images where there should be no signal. How do we tackle the background noise in ICS analysis? The underlying script takes the average intensity outside of the "cell" area and subtracts this value from the pixels in the cell area. The corrected pixels from the cell area is then analyzed with ICS, and the resulting CF is shown on left in Figure 15G. Whether we fit with $G(0,0)$ (Fig 15G, middle panel) or without (Fig 15G, right panel), the number density recovered is drastically improved.

Q8 for the learner

If you were to perform the same simulations (with or without cell mask) and apply TICS for diffusion and flow recovery, how would diffusion coefficient recovered compare with set value of 0.01 $\mu m^2\ s^{-1}$? Does the correction for background noise improve the measured value of D? When applying TICS, set the maximum τ from 20 to 100 to increase number of τ values and bias the fit toward larger temporal lags.

H. ICS simulation case 8: diffusion coefficient recovery in presence of fluorophores photobleaching

In this section, we will demonstrate how photobleaching, which is one of the fundamental properties of fluorescent labels, such as

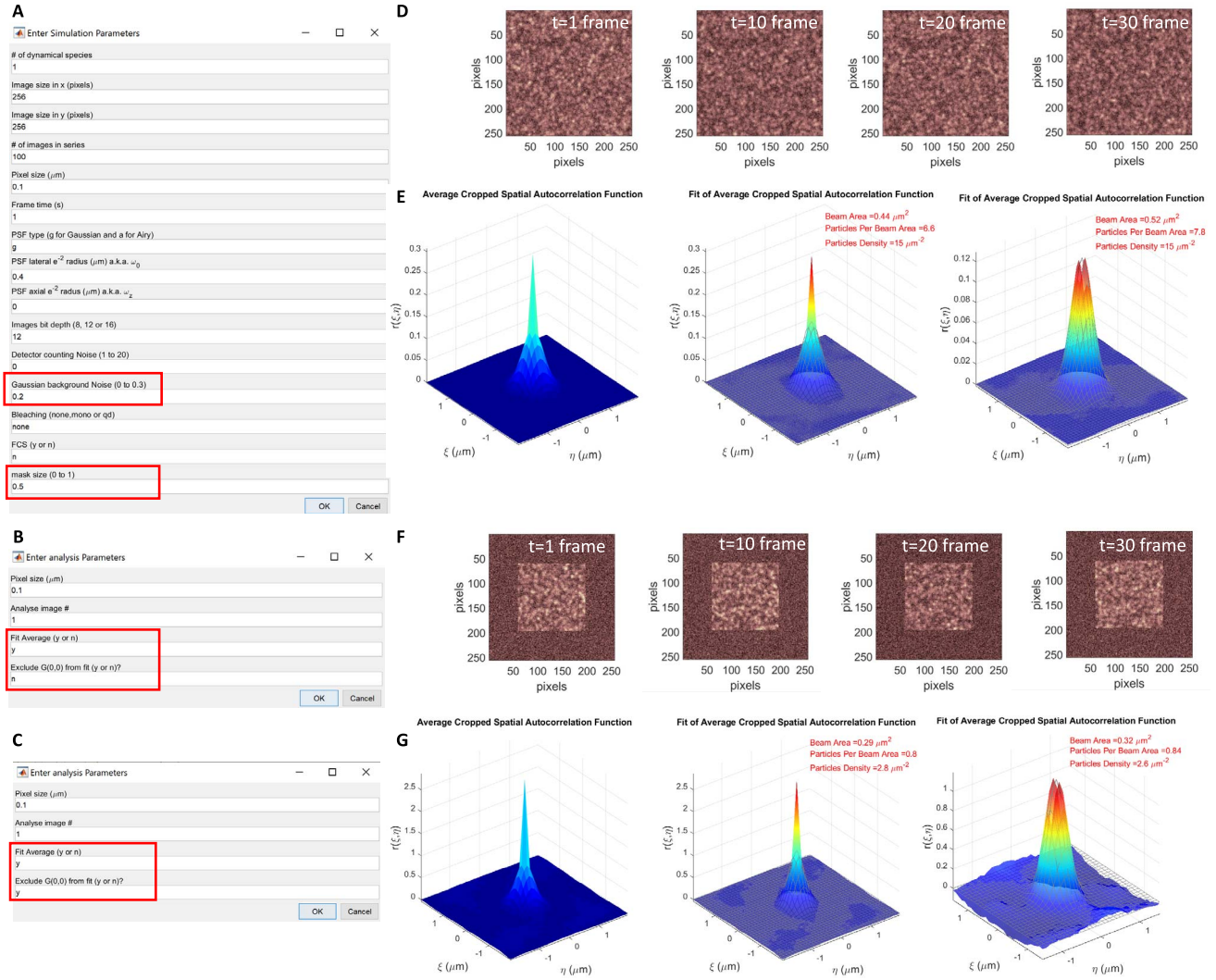

Fig 15. Input dialogues for simulating a diffusing population in ICS experiment in presence of background noise. (A) Inputs for image series simulation in which the background noise parameter is set to a nonzero value of 0.2 (to red rectangle). For data shown in (F) and (G), we set the mask parameter also to a nonzero value, 0.5 in this example (second red rectangle). (B) Input parameters for ICS analysis to apply ICS to an average CF and to include the $G(0,0)$ value in the fit. (C) Input parameters for ICS but here setting the $G(0,0)$ value to y, to exclude it from the fit. (D) Frames 1, 10, 20, and 30 of time series simulated. This series is identical to section VI.B, except that here we added background noise, of 0.2, to the image series. (E) Raw average CF (left), fitted with (middle), and without (right) $G(0,0)$ point included. Red text displays summary of recovered parameters from the fit. (F) Frames 1, 10, 20, and 30 of time series simulated with and active (inner square) and a background (outside of the square) areas. This series mimics situation where an active area could be pixels within a cell and background area contain pixels outside of cells. (G) ICS results for data simulated as shown in (F). Left, center, and right represent the average CD within active area, postfitting, including $G(0,0)$ point and excluding $G(0,0)$ in the fit.

dyes, can lead to bias in measured parameters from TICS, such as the number density. Indeed, to generate image data, we need to expose the fluorophores, which tag proteins of interest to the source of light, a fluorescent lamp or a laser light. In either case, increasing the intensity of light source increases the amount of fluorophores excited and also number of cycles of excitation–emission, which results in an overall amplified signal. This is, of course, the beneficial side of increasing the light source intensity. Unfortunately, there are negative aspects of this experimental control, beside potential phototoxicity and cell death. One of them is that the fluorescent dyes undergo an irreversible conversion to a dark state. In other words, fluorophores turn off and remain off for the time longer than the experimental setting. This

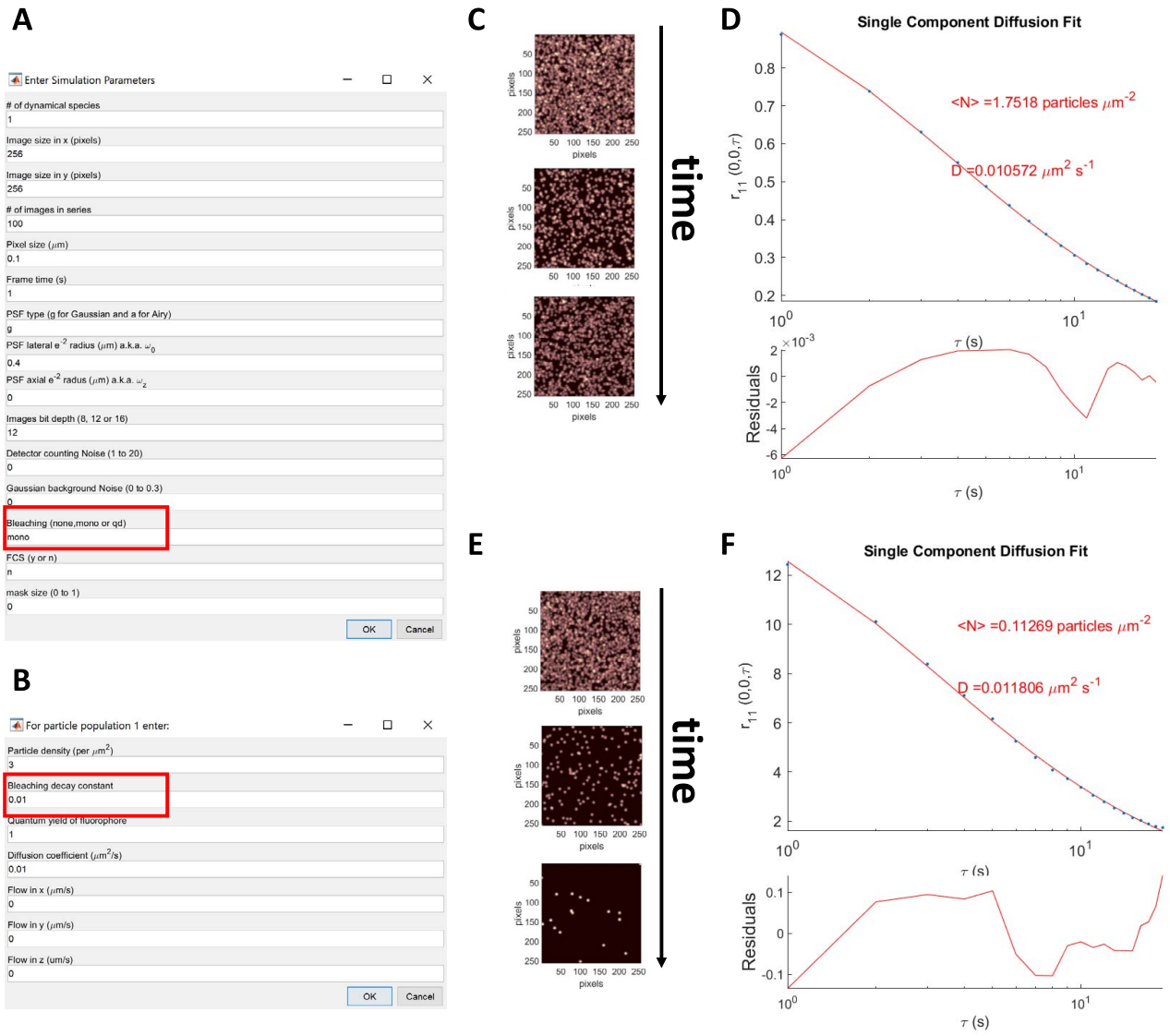

Fig 16. Input dialogues for simulating a diffusing population in ICS experiment in presence of photobleaching. (A) Inputs for image series simulation in which the bleaching parameter is set to mono (red rectangle). For data shown in (F) and (G), we set the mask parameter also to a nonzero value, 0.5 in this example (second red rectangle). (B) Prompt for particle population simulation. Set the bleaching decay constant to 0.01 s^{-1} (red rectangle). (C) Frames 1, 50, and 100 of time series simulated. This series is identical to section VI.B, except that here we have a photobleaching of particles at rate of 0.01 s^{-1} in the image series. (D) TICS ACF for data in (C). Circle showing the calculated ACF and red line showing the fit to the 1 component diffusion in 2D. Red text displays the fitted parameters, number density, and diffusion coefficient. (E) Frames 1, 50, and 100 of time series simulated. This series is identical to section VI.B, except that here we have a photobleaching of particles at rate of 0.05 s^{-1} in the image series. (D) TICS ACF for data in (E). Circle showing the calculated ACF and red line showing the fit to the 1 component diffusion in 2D. Red text displays the fitted parameters, number density, and diffusion coefficient.

has an effect on both the number densities measured, as well as dynamics from ICS and TICS. We will explore how in the example that follows.

Let us simulate the data as we did in section VI.B, but this time, set the bleaching to mono, which will add the photobleaching to the image series, in a monoexponential decay fashion (Fig 16A). When specifying the particle population parameters, use the settings as shown in Figure 16B, making the decay rate of bleaching equal to 0.01. This will generate an image time series that will show a decrease of number of visible particles in time, as described by set rate (Fig 16C). If we were to run TICS analysis on this dataset and then apply a single

component diffusion fit, because that is what we know we simulated, we will generate fit as shown in Figure 16D. Clearly the number density recovered lower than the set value of 3 particles per micrometer squared, as one would expect. On the other hand, there are enough particles in frames that still produce the characteristic temporal fluctuations of the order $\tau_D = \omega_0^2/4D = 4$ seconds, which coherently decorrelate and recover the expected diffusion coefficient. If we increase the rate from 0.01 to 0.05, we will generate data, as shown in Figure 16E. TICS analysis will result in ACF that, when fit, will still underestimate the number densities but by order of magnitude, while estimating still quite accurately the diffusion coefficient (Fig 16F).

Although we cannot directly remedy the images affected by photobleaching, there have been correction in both FCS and TICS which account for it. We will discuss these further in section VII.

Q9 for the learner

Are there photobleaching rates at which TICS would be an accurate technique to measure diffusion coefficient? How would you determine this rate considering the diffusion time?

VII. DISCUSSION

We hope that the user of these exercises has obtained a good understanding of the basic models and techniques in FFCS. In particular, we hope you have gained insight into how the parameters measured relate to the CFs calculated from the raw fluorescence fluctuations. To gain additional perspective of the scales of diffusion coefficients or flow speed measured in literature, we invite consultation of the table in Appendix D. Note that wide variability of the speed of some molecules or organelles have, depending on their system context. For example, adhesion molecules, such as integrins or paxilins, will exhibit intermediate speeds of $\sim$1 to 5 μm min^{-1} in the context of cellular gripping to substrate during cellular migration (22, 23, 25). Compare this to several orders of magnitude lower speed of the corneal stem cells during the migration in the context of wound healing (30, 31). Of course, the cellular speed during migration will also depend on several environmental factors, such as substrate stiffness. Nevertheless, these examples demonstrate that events within cells often occur on much faster timescales to facilitate a cellular task at a slower rate, such as cellular migration. Similarly, during cell division, a new cell membrane or for plant cells, a cell wall, is built by vesicles fusion (29) and active transport of these happens relatively quickly at a rate of $\sim$1 to 10 μm min^{-1}. Note that the same molecule or organelle, such as actin filaments, can flow or assemble and disassemble at different rates, depending on the cellular or role context. Indeed, when T cells are activated and membrane proteins, such as T-cell receptors, are corralled and organized in functional units, actin filaments flow at a rate of $\sim$1–5 μm min^{-1} (26). On the other hand, in the context of dendritic cells poking through dense tissues with organelles, such as podosomes, actin organizes in these organelles that assemble at an order of magnitude slower rate (28). We hope that the reader, by gaining a greater understanding of FFCS approaches, has gained a greater appreciation of the complexity of molecular and cellular dynamics and how they are interrelated.

During the exercises performed, we inspected the residuals of the fit that inform of the degree of model fits to the CF data. To further appreciate the topic of the biases and standard deviation in FCS measurement, we refer the readers to the following literature (19, 32–36). Note that it will not always be possible to fit a model to the data, especially if the CFs are very noisy. In section VI.G, we explored how the background noise can skew the ICS CF so that it does not have a single 2D Gaussian shape. In this scenario, we can often correct for this type of noise and avoid $G(0,0)$ in the fitting. However, there are instances in which spatiotemporal sampling is insufficient or the CF is so noisy that it is not possible to correct the data or CF. The phasor analysis approach is one method that may overcome this issue. It was developed originally for fluorescence lifetime data characterization but was applied to both FCS (37) and more recently ICS (38) data, to

characterize the CFs without resorting to nonlinear fitting. Indeed, this approach allows us to characterize and group CFs without fitting, even in the presence of significant noise, while any attempt of nonlinear fitting would be difficult or rather impossible. For users interested in exploring more how phasor analysis work, but also for an integrated platform for single molecule and ensemble approaches (ICS, RICS, and FCS), we suggest the MATLAB-based free software by the name PAM (39). For a software that integrates most of the correlation spectroscopy approaches, please consult the SimFCS Web page (http://www.globalssoftware.com).

Note that some biases can be corrected on raw data and some accounted for when fitting CFs. A careful experimenter will try to minimize the biases and account for them in acquisition and analysis of data. When impossible to avoid biases, it is absolutely necessary to have sufficient amount of control data and measure all the conditions (control and others) with same systematic biases, so measured values of densities, diffusion coefficients, flow parameters, or others can be compared. After all, it is difficult to measure an absolute value of anything, as measurement errors are inevitable, but it is essential to track these biases and be able to account for them when comparing the measured values.

Note that we did not look at more complex scenarios, such as with multiple dynamic populations, with different quantal brightness occur. This could be a case in which a monomer protein aggregates into a higher oligomer. One of the complexities that arise from this measurement is that both the monomer and oligomer state give rise to fluctuations. Given that the CF amplitude scales as the density squared and is directly proportional with the brightness, it would require 16 times more of monomer than tetramer to produce equal contribution to the CF amplitude. Therefore, higher oligomers can mask and even dominate the CFs. Luckily, there are a few extensions to the techniques that occurred over years, separating contributions from different oligomers in stationary image data (40–42) and in dynamic data (43, 44). Another way to circumvent the problem is to label proteins with photoactivable fluorescent proteins, and depending of subset of fluorophores being active, measure CF from only visible population (45). Even multiple flows were successfully detected within the same region of interest through extensions of STICS (46, 47).

In the current article, we covered only the cases in which a single channel acquisition (imaging) occurs and did not explicitly consider the cases of 2-color labeling. Indeed, if we had a scenario in which 2 potentially interacting proteins are labeled with 2 spectrally distinct fluorophores, then we could apply either FCCS, ICCS, or STICCS to investigate the interaction between these proteins and the codynamics (3, 19, 20, 35).

When we looked at cases in which particles were simulated to diffuse within system, we assumed that they underwent free diffusion. In reality, most proteins and organelles in cells diffuse anomalously or are confined by the surroundings. There has been a body of work in last 10 years or so in both FCS and ICS extensions to account for this modality of particle motion. In particular, the FCS beam was shaped and for every beam size FCS ACF was recorded (48, 49). Plotting the characteristic decay time of ACF for each of these beam volumes versus the squared radius of volume led to a phenomenologic relation called diffusion law, which is the equivalent of MSD from particle tracking. The MSD, usually by its trend versus temporal lag, instructs us on what type of confinement or obstacle caused the anomalous or confined random walk. Extracting the equivalent of MSD from the CF was done in the past by using STICS (25, 50) or equivalent imaging correlation approach (51) and even allowed for diffusion coefficient mapping (25, 45), as we saw in the theoretic development leading up to Eqs. 10 and 11 and as shown in spreading STICS CF in Figure 14D.

Similarly, measurement of diffusion coefficient without any bias of the fluorophore's photophysics was explored in Fourier space of full spatiotemporal CF, through another ICS extension termed *k*-space ICS (kICS) (52). This

technique exploits Fourier space to separate dynamical and photophysics components of CF and furthermore was applied to measure binding kinetics (53) and confined membrane protein dynamics (54, 55). Both kICS and STICS explore more than a single spatial position, which makes these techniques less sensitive in recovering the dynamical parameters, such as diffusion coefficient, in presence of photobleaching or other fluorophore intermittent emission. As explored in the last section of this article, measuring fluctuation in time from a single pixel, as in TICS or FCS, leads to an ACF that is prone to errors. Indeed, there is a bias in dynamic parameters measured if the characteristic time of photobleaching or blinking is shorter than the average diffusion or flow time. On the other hand, multifoci FCS, line scan analysis through pair CF (44) or beam-varying FCS (48, 49) probe more than one spatial position and correlate spatiotemporally. Other corrections for photobleaching have been explored, such as signal detrending, and in the case of TICS analysis, accounting for the photobleaching decay contribution to the CF (56). For a good introduction to kICS and known applications, we recommend that the user consults the book chapter (57). Also, for an example of how kICS can be applied, as demonstrated through a video journal, we suggest (58).

In summary, FFCS techniques have been useful from the onset some 50 years ago and have grown in number and usage ever since then. We hope that the reader was able to appreciate this tremendous body of work and will find a way of applying some of the existing tools to future research. If the reader is unable to find the right FFCS tool in the toolbox, then we hope the reader will make his or her own extension and share with the greater FFCS community!

SUPPLEMENTAL MATERIAL

The MATLAB scripts are available at https://doi.org/10.35459/tbp.2019.000143.S1.

ACKNOWLEDGMENTS

We thank Paul W. Wiseman from Departments of Physics and Chemistry at McGill University (Montreal, Canada), David L. Kolin from Brigham and Women's Hospital (Boston, MA), and Santiago Costantino from Department of Ophthalmology Biomedical Engineering Institute (Montreal, Canada) for sharing the original scripts that led to the implementation of exercises in the article.

AUTHOR CONTRIBUTIONS

EP and RMW designed the project. EP tested all exercises, consolidated the scripts, and wrote the manuscript.

APPENDIX A. DERIVATION OF EQ. 3

In this appendix, we will see how we obtain Eq. 3 from the generalized FCS ACF expression (Eq. 1). The similar derivation would lead to Eqs. 4 and 6–9. First, let us define the observation volume spatial function:

$$I(r) = I_0 e^{-2\frac{x^2+y^2}{\omega_0^2}} e^{-2\frac{z^2}{\omega_z^2}} \tag{A1}$$

Let us assume for simplicity that we have a single population, $M = 1$, without loss of generality as terms for other population would be equivalent and summing up, then Eq. 1 reduces to

$$G(\tau) = \frac{g^2 \int_{-\infty}^{+\infty} I(r) I(r') \langle \delta c(r,0) \delta c(r',\tau) \rangle dr dr'}{\left(g \langle c \rangle \int_{-\infty}^{+\infty} I(r) dr \right)^2} \tag{A2}$$

where $\langle c \rangle$ is the equilibrium concentration of particles, which is assumed constant. Also, assuming that particles are freely diffusing in 3D with the diffusion coefficient D, then the density–density ACF, $\langle \delta c(r,0) \delta c(r',\tau) \rangle$, can be defined as

$$\langle \delta c(r,0) \delta c(r',\tau) \rangle = \frac{\langle c \rangle}{(4\pi D\tau)^{\frac{3}{2}}} e^{\frac{-(r-r')^2}{4D\tau}} \tag{A3}$$

This last expression comes from solving the diffusion equation, which same as Eq. 2 but with only first term on the right-hand side and assuming the initial condition $c(r, 0) = \langle c \rangle$. Then, Eq. A2 writes

$$G(\tau) = \frac{\int_{-\infty}^{+\infty} e^{-2\frac{x^2+y^2}{\omega_0^2}} e^{-2\frac{z^2}{\omega_z^2}} e^{-2\frac{x'^2+y'^2}{\omega_0^2}} e^{-2\frac{z'^2}{\omega_z^2}} e^{\frac{-(r-r')^2}{4D\tau}} dx dy dz dx' dy' dz'}{\langle c \rangle (4\pi D\tau)^3 \left(\int_{-\infty}^{+\infty} e^{-2\frac{x^2+y^2}{\omega_0^2}} e^{-2\frac{z^2}{\omega_z^2}} dx dy dz dx' dy' dz' \right)} \tag{A4}$$

where we cancelled $\langle c \rangle$ from numerator and d^2. Here $r - r' = (x - x') + (y - y') + (z - z')$ define the dummy variables of integration r and r'. The trick to integrate all of the spatial integrals is to group all the terms together, say for dummy variable x' and then one of the definitions of the integral of Gaussian function:

$$\int_{-\infty}^{+\infty} e^{-a(x+b)^2} dx = \sqrt{\frac{\pi}{a}} \tag{A5}$$

or

$$\int_{-\infty}^{+\infty} e^{-ax^2+bx+c} dx = \sqrt{\frac{\pi}{a}} e^{\frac{b^2}{4a}+c} \tag{A6}$$

Combining the terms together and completing the squares simplifies all of the exponentials in the numerator, leading to the final solution for FCS ACF for 3D free diffusion:

$$G(\tau) = \frac{1}{\pi^{\frac{3}{2}}\omega_0^2\omega_z}\frac{1}{(1+\frac{\tau}{\tau_D})}\frac{1}{\sqrt{1+\left(\frac{\omega_0}{\omega_z}\right)^2\frac{\tau}{\tau_D}}} \quad \text{(A7)}$$

For the measurement from a membrane that is perpendicular to the axial direction of acquisition, we can assume that $\omega_z - > 0$, and denominator in Eq. A3 has power of 1, which, in turn, converts Eq. A7 to

$$G(\tau) = \frac{1}{\pi\omega_0^2}\frac{1}{\left(1+\frac{\tau}{\tau_D}\right)} \quad \text{(A8)}$$

This is just the Eq. 3, where $M = 1$, for a single dynamic population. We can easily see why sum of freely diffusing populations would lead to an FCS ACF that is a sum of such terms.

Similar type of integration over spatial coordinates lead to the Eq. 7 in TICS. For flow model, one would need to find a similar density–density ACF, as shown in Eq. A3, but in case of flowing particles. To obtain this, one would need to solve a partial differential equation, with the initial condition of constant flow $\vec{v}$ and with the second term alone on the right-hand side of Eq. 2.

APPENDIX B. SYSTEM REQUIREMENTS

(a) Any platform supporting MATLAB (preferably the latest version).

(b) There are no hardware requirements per se. Processor speed will play a large role in the analysis time and the amount of system RAM will dictate the maximum size of the image series that can be analyzed.

APPENDIX C. ANSWERS TO THE QUESTIONS

Answer to Q1

From Figure 6B,C, residuals in range 1 to 10 s show that 2D diffusion fit model did not fit the FCS ACF, as well as the 3D Diffusion fit. The simulated data was generated by using $D = 0.03$ $\mu m^2\ s^{-1}$ and particle density = 1.5 particles per micrometer squared. From Figure 6, we can see that the most accurate estimate of these parameters was obtained from the 3D diffusion fit, where recovered values were 0.032 $\mu m^2\ s^{-1}$ and 1.6 particles per micrometer squared. It is possible that if a 2-component diffusion model was fit, with 5 fit parameters (2 amplitudes, 2 decay rates, and 1 offset), it would lead to even smaller residuals in the temporal lag range of 10 to 100 s. Nevertheless, it is obvious that there are no 2 decays (dynamic populations) present in the ACF, hence making the choice of 2-component fit incorrect, independent of how low resulting residuals are. Similarly, χ^2 or R^2, which are other metrics for goodness of fit, might give better results for 2-component fit, but correct metric in this case would be the adjusted R^2, as it takes into account the number of fitted parameters for a given model. In other words, fitting model with more parameters is not the right solution if it is used just to improve the goodness of fit and caution should be in order when choosing the fitting model.

Answer to Q2

The set particle flow in this FCS simulation was $(v_x, v_y, v_z) = (0.1,–0.1,0.05)$ $\mu m\ s^{-1}$, giving the total speed of $\sqrt{01^2 + (-01)^2 + 0.05^2} = 0.15$ $\mu m\ s^{-1}$. Also, the set density of particles was 1.5 particles per micrometer squared. Comparing the 2 fitted model on Figure 7B,C, it is clear that the single component flow fit better follow the trend of simulated ACF in this case. The recovered speed and particles densities of 0.15 $\mu m\ s^{-1}$ and 1.8 particles per micrometer squared are very close to the set values.

Answer to Q3

In this simulation scenario, 1 diffusing population ($D = 0.05$ $\mu m^2\ s^{-1}$) and 1 flowing population $(v_x, v_y, v_z) = (0.07,–0.05,0.04)$ $\mu m\ s^{-1}$ or $v = 0.0948$ $\mu m\ s^{-1}$ were simulated with densities of 1.5 and 0.7 particles per micrometer squared, respectively. Fitting a model incorporating the sum of 3D diffusing and another flowing population leads to ratio of densities of $N_D/N_v = 2.09$ (compared with $1.5/0.7 = 2.14$), diffusion coefficient of 0.051 $\mu m^2\ s^{-1}$), and speed of 0.095 $\mu m\ s^{-1}$. These recovered values are in very good agreement with set values and attempting to fit any other model presented in early sections of FCS would not lead to correct estimates of particle diffusion coefficient, flow speed and ratio of their densities. In the example simulated, the diffusion time was $\tau_D = \omega_0^2/4D = 0.8$ s, therefore requiring the sampling time to be at least half of that value. For this reason, we set the integration time to 0.1 s and consequently extended the simulation to 50,000 samplings or 5,000 s in total. Also, given that flow speed leads to the characteristic decay at $\tau_f = \omega_0/v = 4$ s, we want to have the maximum temporal lag extending to at least 10 s, so the fit can recover the second decay due to the flow. In turn, given that the FCS ACF becomes noisier for larger temporal lags (see lags 100 s and above of ACF in Fig 8D), we wanted to have enough sampling so that ACF in the temporal lags 0 to 100 s is well defined for fitting. That is how on the basis of characteristic decay times, which are also characteristic transit times through the observation volume of any dynamic population involved, τ_D or τ_f, that we determine the total length of acquisition.

Answer to Q4

If we were to rerun ICS analysis on the same dataset, but this time, choose to take the temporal average of the ICS ACF and fit it with the 2D Gaussian, the estimate of particle number density would improve. Indeed, comparing the results from Figure 9D, where we have 3.51 particles μm^{-2} while when we averaged the ICS ACF from all the frames, as shown in Figure 9F, we obtain 3.07 particles per micrometer squared, which is much closer estimate of set density (3 particles per micrometer squared). It is a consequence of the averaging out of noise peaks that occur at spatial lags larger than few pixels from the main peak in ICS ACF. Although those spurious peaks from ACF of each image average out, the main central peak becomes amplified as it occurs in every frame ACF. Note that if particles in the image are subdiffraction in size, then the waist of ICS ACF ω_0 is a good estimate of the microscope effective PSF lateral radius, making ICS a very quick way of measuring your PSF lateral extent.

Answer to Q5

Diffusion fit to TICS ACF produced quite good estimate of simulated particles density and diffusion coefficient (<1% error). On the other hand, trying to fit a 1 component flow model to the data resulted in very large residuals as shown in

Figure 10C. Obviously, this model does not fit the TICS ACF well for this simulated example.

Answer to Q6

The recovered flow value from STICS analysis was in very good agreement with set value in simulation. The collective information from spatiotemporal correlation and position of STICS CF peak at several lags is what makes this methodology robust. If one or few temporal lags gave erroneous CF, which, in turn, would deviate from the linear trend, shown in Figure 12F, the overall linear fit to extract speeds in *x* and *y* directions would still recover approximately same values. In the example of immobile population bias, we can see how an extra peak in STICS CF affected the recovery of flow value and how the immobile filtering fixed the problem. In case you have multiple populations flowing, you will obtain multiple STICS CF peaks moving in same direction and at same rate as the underlying particle flow. To characterize these complex dynamics, we point the reader to the literature examples mentioned in section VII, such as the velocity landscape correlation (47).

Answer to Q7

The flow recovered by STICS in both *x* and *y* directions was within $<1\%$ error, even in this case in which the particles were undergoing simultaneous flow and diffusion. Interestingly, the STICS CF was spreading and decreasing in amplitude at the same time that it was translating due to the flowing of the particles. If the user refers to the Eqs. 10 and 11, it can be seen that the increase in the CF width squared is proportional to the diffusion coefficient of particles. Therefore, a linear trend in $\omega_0^2(\tau)$ versus τ has a slope that is equal to the 4 times diffusion coefficient.

Answer to Q8

Applying TICS without background noise correction (or without mask of 0.5) resulted in diffusion coefficient of $\sim$0.04 $\mu m^2\ s^{-1}$. Simulating the masked data and the correction for background noise should improve the recovered diffusion coefficient value to about 0.09 $\mu m^2\ s^{-1}$.

Answer to Q9

If the rate of diffusion is faster than the photobleaching, the particles will, on average, have time to transit the observation volume, before being in the "off" state. This rate, for example simulated is $1/\tau_D = 0.25 s^{-1}$. Because that rate is much higher than either of simulated photobleaching rates, we were safe to estimate *D* by using fitting of TICS ACF. If on the other hand, our photobleaching rate was higher than 0.4 s^{-1}, then, on average, the particle time "on" would be shorter than the diffusion time and effectively would shift TICS curve to the left, suggesting faster diffusion then the set value. Any single spatial point acquisition approach, such as FCS, will suffer from this bias.

APPENDIX D. Examples of experimentally measured values of dynamic parameters.

Protein and cell type	Parameter	Value ($\mu m^2\ s^{-1}$ for *D* or $\mu m\ min^{-1}$ for *v*)	Technique	Reference
CFTR in pHBE cell membrane	*D*	0.005–0.015	kICS	54, 55
α5-Integrin in CHO-K1 cell membranes	*D*	0.0095–0.0097	kICS	52
Lipids in model membrane	*D*	0.3–5	ITIR-FCS	51
TfR in CHO-K1 cell membrane	*D*	0.2–0.7	STICS (iMSD)	50
GFP-GPI,GFP-Thy1 and GFP-TfR in COS-7 cell membrane	*D*	0.5–1.0	Beam varying FCS	48
GFP-αLβ2 integrin and mCherry-paxillin in CHO-B2 cell	*v*	3–4	*v*ICS	45
GFP-αLβ2 integrin and mCherry-paxillin in U2OS cell	*v*	1	STICCS	25
Lck-mEOS2 in JCAM T-cell membrane	*D*	0.1–1	paSTICS	44
hIR-GFP in CHO-K1 cells	*D*	0.2–1	phasor FCS	37
Corneal stem cell migration	*v*	0.001–0.2	STICS	30, 31
Vesicles delivery to a plant cell wall	*v*	1–10	STICS	29
LifeAct-GFP in podosomes of DC cells on glass	*v*	0.1-0.2	STICS	28
β-Tubulin C-terminal tails in NCI-H460 cells	*v*	10-50	STICCS	27
F-Actin in T-cell activation	*v*	1-5	STICS	26
α5-Integrin in CHO-B2 cells	*D*	0.0004-0.005	TICS	24
α5-Integrin it cell edge of CHO-B2 cells	*v*	40	TICS	24

CHO-K1 or CHO-B2: Chinese Ovary Cancer cell lines, CFTR: Cystic Fibrosis Receptor, COS-7: Monkey kidney fibroblast-like cell, GFP: Green Fluorescent Protein, GPI: Glycosylphosphatidylinositol, HBE: Human Bronchial Epithelial cells, hIR: HEAT-like repeat protein, JCAM: lck deficient mutant of T-cell Jurkat line, Lck: lymphocyte-specific protein tyrosine kinase, LifeAct: Genetically encoded tag for filamentous F-actin, NCI-H460: Human Non Small Lung Carcinoma cells, TfR: Transferrin Receptor, Thy1 (CD90): THYmocyte differentiation antigen 1, U2OS: Human bone osteosarcoma epithelial cells.

REFERENCES

1. Magde, D., E. L. Elson, and W. W. Webb. 1972. Thermodynamic fluctuations in a reacting system—measurement by fluorescence correlation spectroscopy. *Phys Rev Lett* 29(11):705–708.
2. Elson, E. L., and D. Magde. 1974. Fluorescence correlation spectroscopy. I. Conceptual basis and theory. *Biopolymers* 13:1–27.
3. Schwille, P., F. J. Meyer-Almes, and R. Rigler. 1997. Dual-color fluorescence cross-correlation spectroscopy for multicomponent diffusional analysis in solution. *Biophys J* 72:1878–1886.

4. Magde, D., W. W. Webb, and E. L. Elson. 1978. Fluorescence correlation spectroscopy. III. Uniform translation and laminar flow. *Biopolymers* 17:361–376.
5. Aragon, S. R. and R. Pecora. 1976. Fluorescence correlation spectroscopy as a probe of molecular dynamics. *J Chem Phys* 64:1791–1803.
6. Widengren, J., J. Dapprich, and R. Rigler. 1997. Fast interactions between Rh6G and dGTP in water studied by fluorescence correlation spectroscopy. *Chem Phys* 216(3):417–426.
7. Widengren, J., U. Mets, and R. Rigler. 1999. Photodynamic properties of green fluorescent proteins investigated by fluorescence correlation spectroscopy. *Chem Phys* 250(2):171–186.
8. Korlach, J., P. Schwille, W. W. Webb, and G. W. Feigenson. 1999. Characterization of lipid bilayer phases by confocal microscopy and fluorescence correlation spectroscopy. *Proc Natl Acad Sci U S A* 96(15):8461–8466.
9. Elson, E. L. 2011. Fluorescence correlation spectroscopy: past, present, future. *Biophys J* 101:2855–2870.
10. Radek, M., and T. Wholand. 2014. Recent applications of fluorescence correlation spectroscopy in live systems. *FEBS Lett* 588:3571–3584.
11. Petersen, N. O. 1986. Scanning fluorescence correlation spectroscopy. I. Theory and simulation of aggregation measurements. *Biophys J* 49:809–815.
12. Petersen, N. O., P. L. Hoddelius, P. W. Wiseman, O. Seger, and K. E. Magnusson. 1993. Quantitation of membrane receptor distributions by image correlation spectroscopy: concept and application. *Biophys J* 65(3):1135–1146.
13. Huang, Z., and N. L. Thompson. 1996. Imaging fluorescence correlation spectroscopy: nonuniform IgE distributions on planar membranes. *Biophys J* 70(4):2001–2007.
14. Wiseman, P. W., P. Hoddelius, N. O. Petersen, and K. Magnusson. 1997. Aggregation of PDGF-/3 receptors in human skin fibroblasts: characterization by image correlation spectroscopy (ICS). *FEBS Lett* 401:43–48.
15. Petersen, N. O., C. Brown, A. Kaminski, J. Rocheleau, M. Srivastava, and P. W. Wiseman. 1998. Analysis of membrane protein cluster densities and sizes in situ by image correlation spectroscopy. *Faraday Discuss* 111:289–305.
16. Wiseman, P. W., and N. O. Petersen. 1999. Image correlation spectroscopy. II. Optimization for ultrasensitive detection of preexisting platelet-derived growth factor-beta receptor oligomers on intact cells. *Biophys J* 76(2):963–77.
17. Srivastava, M., and N. O. Petersen. 1996. Image cross-correlation spectroscopy: a new experimental biophysical approach to measurement of slow diffusion of fluorescent molecules. *Methods Cell Sci* 18:47–54.
18. Wiseman, P. W., J. A. Squier, M. H. Ellisman, and K. R. Wilson. 2000. Two-photon image correlation spectroscopy and image cross-correlation spectroscopy. *J Microsc* 200:14–25.
19. Santiago, C., J. Comeau, D. L. Kolin, and P. W. Wiseman. 2005. Accuracy and dynamic range of spatial image correlation and cross-correlation spectroscopy. *Biophys J* 89:1251–1260.
20. Comeau, J., S. Costantino, and P. W. Wiseman. 2006. A Guide to accurate colocalization measurements. *Biophys J* 91(12):4611–4622.
21. Srivastava, M., and N. O. Petersen. 1998. Diffusion of transferrin receptor clusters. *Biophys. Chem*., 75:201–211.
22. Brown, C. M., B. Hebert, D. L. Kolin, J. Zareno, L. Whitmore, A. F. Horwitz, and P. W. Wiseman. 2006. Probing the integrin-actin linkage using high resolution protein velocity mapping. *J Cell Sci* 119:5204–5214.
23. Hebert, B., S. Costantino, and P. W. Wiseman. 2005. Spatiotemporal image correlation spectroscopy (STICS) theory, verification, and application to protein velocity mapping in living CHO cells. *Biophys J* 88:3601–3614.
24. Wiseman, P. W., C. M. Brown, D. J. Webb, B. Hebert, N. L. Johnson, J. A. Squier, M. H. Ellisman, and A. F. Horwitz. 2004. Spatial mapping of integrin interactions and dynamics during cell migration by image correlation microscopy. *J Cell Sci* 117(23):5521–5534.
25. Toplak, T., E. Pandzic, L. Chen, M. Vicente-Manzanares, A. R. Horwitz, and P. W. Wiseman. 2012. STICCS reveals matrix-dependent adhesion slipping and gripping in migrating cells. *Biophys J* 103(8):1672–1682.
26. Ashdown, G., G. Burn, D. J. Wiliamson, E. Pandzic, R. Peters, M. Holden, H. Ewers, L. Shao, P. W. Wiseman, and D. Owen. 2017. Live-cell super-resolution reveals F-actin and plasma membrane dynamics at the T cell synapse. *Biophys J* 112:1703–1713.
27. Parker, A. L., W. S. Teo, E, Pandzic, J. J. Vicente, J. A. McCarroll, L. Wordeman, and M. Kavallaris. 2018. β-tubulin carboxy-terminal tails have isotype-specific roles on microtubule dynamics in human cells. *Life Sci Alliance* 1(2):e201800059.
28. Maddens, M. B. M., E. Pandzic, J. A. Slotman, D. Guillet, B. Joosten, S. Mennens, L. M. Paardekooper, A. B. Houtsmuller, K. Van den Dries, P. W. Wiseman, and A. Cambi. 2016. Actomyosin-dependent dynamic spatial pattern of cytoskeletal components drive mesoscale podosome organization. *Nat Commun* 7:13127.
29. van Oostende-Triplet, C., D. Guillet, T. Triplet, E. Pandzic, P. Wiseman, and A. Getimann. 2017. Vesicle dynamics during plant cell cytokinesis reveals distinct developmental phases. *Plant Physiol* 174(3):1544–1558.
30. Park, M., A. Richardson, E. Pandzic, R. M. Whan, S. L. Watson, D. Wakefield, and N. Di Girolamo. 2019. Visualizing the contribution of keratin-14^{+} limbal epithelial precursors in corneal wound healing. *Stem Cell Rep* 12(1):14–28.
31. Park, M., A. Richardson, E. Pandzic, E. P. Lobo, J. G. Lyons, and N. Di Girolamo. 2019. Peripheral (not central) corneal epithelia contribute to the closure of an annular debridement injury. *Proc Natl Acad Sci U S A* 116(52):26633–26643.
32. Qian, H. 1990. On the statistics of fluorescence correlation spectroscopy. *Biophys Chem* 38:49–57.
33. Kask, P., R. Günther, and P. Axhausen. 1997. Statistical accuracy in fluorescence fluctuation experiments. *Eur Biophys J* 25:163–169.
34. Ulrich, M., T. Wohland, R, Rigler, and H. Vogel. 1999. Resolution of fluorescence correlation measurements. *Biophys J* 76:1619–1631.
35. Wohland, T., R. Rigler, and H. Vogel. 2001. The standard deviation in fluorescence correlation spectroscopy. *Biophys J* 80:2987–2999.
36. Saffarian, S., and E. L. Elson. 2003. Statistical analysis of fluorescence correlation spectroscopy: the standard deviation and bias. *Biophys J* 84:2030–2042.
37. Ranjit, S., L. Lanzano, and E. Gratton. 2014. Mapping diffusion in a living cell via the phasor approach. *Biophys J* 107:2775–2785.
38. Scipioni, L., E. Gratton, A. Diaspro, and L. Lanzano. 2016. Phasor analysis of local ICS detects heterogeneity in size and number of intracellular vesicles. *Biophys J* 111:619–629.
39. Schrimpf, W., A. Barth, J. Hendrix, and D. C. Lamb. 2018. PAM: A framework for integrated analysis of imaging, single-molecule and ensemble fluorescence data. *Biophys J* 114:1518–1528.
40. Rocheleau, J. V., P. W. Wiseman, and N. O. Petersen. 2003. Isolation of bright aggregate fluctuations in a multipopulation image correlation spectroscopy system using intensity subtraction. *Biophys J* 84(6):4011–4022.
41. Sergeev, M., Costantino S., and P. W. Wiseman. 2006. Measurement of monomer-oligomer distributions via fluorescence moment image analysis. *Biophys J* 91(10):3884–3896.
42. Godin, G. A., S. Costantino, L.-E. Lorenzo, J. L. Swift, M. Sergeev, A. Ribeiro da Silva, Y. De Koninck, and P. W. Wiseman. 2011. Revealing protein oligomerization and densities in situ using spatial intensity distribution analysis. *Proc Natl Acad Sci U S A* 108:7010–7015.
43. Digman, M. A., R. Dalal, A. F. Horwitz, and E. Gratton. 2008. Mapping the number of molecules and brightness in the laser scanning microscopes. *Biophys J,* 94:2320–2332.
44. Hinde, E., E. Pandzic, A. Yang, I. H. Ng, D. A. Jans, M. A. Bogoyevitch, E. Gratton, and K. Gaus. 2016. Quantifying the dynamics of the oligomeric transcriptor factor STAT3 by pair correlation of molecular brightness. *Nat Commun* 7:11047.
45. Pandzic, E., J. Rossy, and K. Gaus. 2015. Tracking molecular dynamics without tracking: image correlation of photo-activation microscopy. *Methods Appl Fluoresc* 3(1):014006.
46. Potvin-Trottier, L., L. Chen, A. R. Horwitz, and P. W. Wiseman. 2013. A nu-space for ICS: characterization and application to measure protein transport in live cells. *New J Phys* 15(10):085006. https://doi.org/10.1088/1367-2630/15/8/085006.
47. Pandzic, E., A. Abu-Arish., R. M. Whan, J. W. Hanrahan, and P. W. Wiseman. 2018. Velocity landscapes resolve multiple dynamical populations from fluorescence image time series. *Methods* 140–141:126–139.
48. Wawrezinieck, L., H. Rigneault, D. Marguet, and P. F. Lenne. 2005. Fluorescence correlation spectroscopy diffusion laws to probe the submicron cell membrane organization. *Biophys J* 89:4029–4042.
49. Wawrezinieck, L., F. Conchonaud, O. Wurtz, A. Boned, X.-J. Guo, H. Rigneault, H.-T. He, D. Marguet, and P.-F. Lenne. 2006. Dynamic molecular confinement in the plasma membrane by microdomains and the cytoskeleton meshwork. *EMBO J* 25:3245–3256.
50. Di Rienzoa, C., E. Gratton, F. Beltram, and F. Cardarelli. 2013. Fast spatiotemporal correlation spectroscopy to determine protein lateral diffusion laws in live cell membranes. *Proc Natl Acad Sci U S A* 110:12307–12312.
51. Bag, N., D. Hui Xin Yap, and T. Wholand. 2014. Temperature dependence of diffusion in model and live cell membranes characterized by imaging

fluorescence correlation spectroscopy. *Biochim Biophys Acta Biomembr* 1838(3):802–813.
52. Kolin, D. L., D. Ronis, and P. W. Wiseman. 2006. k-Space image correlation spectroscopy: a method for accurate transport measurements independent of fluorophore photophysics. *Biophys J* 91(8):3061–3075.
53. Brandao, H. B., H. Sangji, E. Pandzic, S. Bechstedt, G. J. Brouhard, and P. W. Wiseman. 2013. Measuring ligand receptor binding rates with k-space image correlation spectroscopy: theory and experimental application. *Methods* 66:273–282.
54. Abu-Arish, A., E. Pandzic, J. Goeppe, E. Matthes, J. W. Hanrahan, and P. W. Wiseman. 2015. Cholesterol modulates CFTR confinement in the plasma membrane of primary epithelial cells. *Biophys J* 109:85–94.
55. Abu-Arish, A., E. Pandzic, D. Kim, H. Wei Tseng, P. W. Wiseman, and J. W. Hanrahan. 2019. Agonists that stimulate secretion promote the recruitment of CFTR into membrane lipid microdomains. *J Gen Physiol* 151(6):834–849.
56. Kolin, D. L., S. Costantino, and P. W. Wiseman. 2006. Sampling effects, noise, and photobleaching in temporal image correlation spectroscopy. *Biophys J* 90(2):628–639.
57. Pandzic, E. and P. W. Wiseman. 2017. Probing membrane heterogeneity with k-space image correlation spectroscopy. In Membrane Organization and Dynamic. A. Chattopadhyay, editor. Springer, Cham, Switzerland, pp. 147–165.
58. Arnspang, E. C., J. S. Koffman, S. Marlar, P. W. Wiseman, and L. N. Nesjsum. 2014. Measurement of diffusion coefficient of EGFP-tagged plasma membrane proteins using k-space image vorrelation spectroscopy. *J Vis Exp* 87:51074.